WL-TR-96-2105

RESEARCH IN STRUCTURAL DYNAMICS AND CONTROL AND AEROPROPULSION

CLARK ATLANTA UNIVERSITY
JAMES P. BRAWLEY DRIVE AT FAIR STREET
ATLANTA GA 30314

MAY 1996

FINAL THE FOR PERIOD 09/01/90 - 09/01-95

Approved for public release; distribution unlimited

AERO PROPULSION AND POWER DIRECTORATE
WRIGHT LABORATORY
AIR FORCE MATERIEL COMMAND
WRIGHT-PATTERSON AIR FORCE BASE, OH 45433-7251

NOTICE

USING GOVERNMENT DRAWINGS, SPECIFICATIONS, OR OTHER DATA INCLUDED IN THIS DOCUMENT FOR ANY PURPOSE OTHER THAN GOVERNMENT PROCUREMENT DOES NOT IN ANY WAY OBLIGATE THE US GOVERNMENT. THE FACT THAT THE GOVERNMENT FORMULATED OR SUPPLIED THE DRAWINGS, SPECIFICATIONS, OR OTHER DATA DOES NOT LICENSE THE HOLDER OR ANY OTHER PERSON OR CORPORATION; OR CONVEY ANY RIGHTS OR PERMISSION TO MANUFACTURE, USE, OR SELL ANY PATENTED INVENTION THAT MAY RELATE TO THEM.

THIS REPORT IS RELEASABLE TO THE NATIONAL TECHNICAL INFORMATION SERVICE (NTIS). AT NTIS, IT WILL BE AVAILABLE TO THE GENERAL PUBLIC, INCLUDING FOREIGN NATIONS.

THIS TECHNICAL REPORT HAS BEEN REVIEWED AND IS APPROVED FOR PUBLICATION.

Alan B. Veg Bali

ALAN B. VEG BALI, PROJ. ENGR.
Fan/Compressor Branch
Turbine Engine Division
Aero Propulsion & Power Directorate

Marvin A. Stibich

MARVIN A. STIBICH, CHIEF
Fan/Compressor Branch
Turbine Engine Division
Aero Propulsion & Power Directorate

Richard J. Hill

RICHARD J. HILL
Chief of Technology
Turbine Engine Division
Aero Propulsion & Power Directorate

IF YOUR ADDRESS HAS CHANGED, IF YOU WISH TO BE REMOVED FROM OUR MAILING LIST, OR IF THE ADDRESSEE IS NO LONGER EMPLOYED BY YOUR ORGANIZATION PLEASE NOTIFY WL/POTF, WRIGHT-PATTERSON AFB OH 45433-7251 TO HELP MAINTAIN A CURRENT MAILING LIST.

Do not return copies of this report unless contractual obligations or notice on a specific document requires its return.

REPORT DOCUMENTATION PAGE	Form Approved OMB No. 0704-0188

1. AGENCY USE ONLY *(Leave blank)*	2. REPORT DATE	3. REPORT TYPE AND DATES COVERED
	MAY 1996	FINAL 09/01/90--09/01/95

4. TITLE AND SUBTITLE
RESEARCH IN STRUCTURAL DYNAMICS AND CONTROL AND AEROPROPULSION

5. FUNDING NUMBERS
C F33615-90-C-2082
PE 64268F
PR 2003
TA 12
WU 10

6. AUTHOR(S)

7. PERFORMING ORGANIZATION NAME(S) AND ADDRESS(ES)
CLARK ATLANTA UNIVERSITY
JAMES P. BRAWLEY DRIVE AT FAIR STREET
ATLANTA, GEORGIA 30314

8. PERFORMING ORGANIZATION REPORT NUMBER

9. SPONSORING/MONITORING AGENCY NAME(S) AND ADDRESS(ES)
AERO PROPULSION AND POWER DIRECTORATE
WRIGHT LABORATORY
AIR FORCE MATERIEL COMMAND
WRIGHT PATTERSON AFB OH 45433-7251
POC: ALAN B. VEG BALI, WL/POTF, (937)255-8210

10. SPONSORING/MONITORING AGENCY REPORT NUMBER
WL-TR-96-2105

11. SUPPLEMENTARY NOTES

12a. DISTRIBUTION AVAILABILITY STATEMENT
APPROVED FOR PUBLIC RELEASE; DISTRIBUTION IS UNLIMITED.

12b. DISTRIBUTION CODE

13. ABSTRACT *(Maximum 200 words)*

The objectives of this research project are to reduce and analyze aeromechanical test data obtained from full scale engine tests at Arnold Engineering Development Center, to investigate the causes for excessive vibration response of the front frame struts of the F110-GE-129 high performance turbofan engine, and to develop analytical and/or empirical models for predicting the conditions under which such high responses occur. The research consists of two parts, namely 1) data processing and analysis, and 2) numerical modeling of fluid flow. Data analysis of existing tapes had been completed and was reported. Accomplishments are: successful development of aircraft engine aeromechanical test data processing capabilities at Clark Atlanta University, development of algorithms to identify damping coefficients from full scale engine test data, completion of analysis of provided data, and unsteady viscous flow analysis for assumed geometry data and flow conditions for the front frame/rotor of the engine under consideration. Finally, implemented an education and training program for students.

14. SUBJECT TERMS	15. NUMBER OF PAGES
Aero-engine data analysis, vibrations, damping, high performance jet engines.	65
	16. PRICE CODE

17. SECURITY CLASSIFICATION OF REPORT	18. SECURITY CLASSIFICATION OF THIS PAGE	19. SECURITY CLASSIFICATION OF ABSTRACT	20. LIMITATION OF ABSTRACT
UNCLASSIFIED	UNCLASSIFIED	UNCLASSIFIED	SAR

TABLE OF CONTENT

1. INTRODUCTION

This report briefly summarizes major work performed on the project entitled "Research in Structural Dynamics and Control and Aeropropulsion" under Contract Number F33615-90-C-2082.

1.1 Objectives

The objectives of this research project are to reduce and analyze aeromechanical test data obtained from full scale engine tests at AEDC, to investigate the causes for excessive vibration response of the front frame struts of the F110-GE-129 high performance turbofan engine, and to develop analytical and/or empirical models for predicting the conditions under which such high responses occur.

1.2 Scope

The research consists of two parts, namely 1). data processing and analysis, and 2). numerical modeling of fluid flow. Data analysis of existing tapes had been completed and was reported in previous quarterly reports. We had waited for availability of geometric profile shapes for the front frame flap, and rotor of first stage of fan. Earlier we had received the geometric profile shapes for the front frame strut. But we did not receive complete information requested. Using the available information and assuming geometric shapes for the flap and rotor, we had continued the process of flow analysis.

1.3 Background

Forced response problems in high performance aircraft engines have remained major obstacles which must be overcome. Over the past several decades, considerable research effort has been devoted to the forced response and fluid-structural instabilities of rotating components such as fan, compressor and turbine rotor systems. Rotating component, such as compressor blade, are susceptible to nonuniform flows generated by inlet distortion, wakes, and pressure disturbances from adjacent blade rows. Large unsteady aerodynamic loads can be experienced by the blades when they pass through these flow nonuniformities or flow defects. When the frequency of these unsteady aerodynamic loads matches the blade natural frequency, blade failures can occur. However, although non-rotating components can also be subjected to unsteady aerodynamic loads which result in high dynamic

stress level in the component, the non-rotating components such as stators and the engine front frame have been validated mainly on the bases of their structural stability and integrity. Little consideration has been given to fluid-structural interactions.

The excessive vibration and the resulting high stress experienced by the front frame struts of the F110-GE-129 caught many people in surprise. At certain conditions, stress on some of the struts significantly exceeded the scope limit for the material, 39.6 KSI, P-P. This limit is fatigue limit based on 10^7 cycles. For the highest stress which occurs at a frequency of 3475 Hz, 10^7 cycles will be exceeded in just 48 minutes. To solve the problem, large amount of experiment which included component test and full scale engine test have been conducted. Based on these tests, the excessive stress levels in the front frame of the F110-GE-129 were due to interactions between the strut's structure and the acoustic field in the duct. Engineering fix which focused on increasing the damping of the front frame strut has been proposed and experimentally validated. Although these measures have increase the structural damping and successfully reduced the dynamic stress well below the scope limit, the physical mechanisms responsible for this problem is yet to be established.

1.4 Outline of Final Report

The outline of this report is as follows: the program objectives and scope are outlined in Chapter 1. Chapter 2 briefly reviewed significant research and training activities under the program. Conclusions from this research program are presented in Chapter 3, which is followed by references in Chapter 4 and appendices.

2. ACCOMPLISHMENTS

2.1 Development of Data Processing Capabilities

The data processing equipment consists of the data reproduction system and the data analysis system. Since the aeromechanical test data provided by AEDC are recorded on 14 tracks of 1 inch wide analog magnetic tapes, the data reproduction system utilized is a HONEYWELL Data Storage Model 101e Portable Tape System. The data analysis system is a 386sx based computer system with adequate software and a Multichannel Spectrum/Network Analyzer--HP 3566A. The tape recorded data are reproduced by the tape system and then acquired by the computer controlled analyzer. The latter then performs analog to digital data conversion, spectral analysis and other operation on the data. In the following, the data processing equipment and the data reduction procedure are discussed.

A HONEYWELL Data Storage Model 101e Portable Tape System is used in the data reproduction. The tape system is a high-performance, IRIG, portable, magnetic tape record/reproduce system with microcomputer control. The system uses 1 inch wide magnetic tape with maximum reel size of 15 inches. It has a 14 track head configuration, among them 12 channels that can be set as FM channels and 2 as direct-record channels. It has a self-contained calibration system and can automatically conduct calibration verification. In this system, data electronics are designed for record/reproduce operation at all eight speeds, from 0.937 to 120 ips, without changing plug-ins. A full selection of FM and direct amplifiers is offered for IRIG intermediate band or wideband applications. A common FM reproduce amplifier is used for all FM modes (IB, WBI, WBII). Electronic flutter compensation and output squelch are standard features of the FM system. Though the system is portable, it provides nearly equal performance as full-size laboratory recorders. For FM record/reproduce, its linearity is 0.5% of full deviation from best straight line through zero. The harmonic distortion is 1.2% maximum for IB and WBI modes and 3.0% for WBII mode. In addition, the operation of the system can also be controlled by an external computer through the RS-232 computer interface.

The core of the data analysis system is the Multichannel, Spectrum/Network Analyzer--HP 3566A. This analyzer is a powerful time and frequency domain measurement tool, which offers features for all types of mechanical testing, including rotating machinery analysis, vibration test, structural analysis and

acoustic noise testing. The analyzer is linked to a 386sx based computer, HP Vectra QS/16S, which controls the operation of the analyzer and performs the data analysis and other operations. The analyzer has 8 channels that acquire data simultaneously, and it can expand to 16 channels if necessary. For fast measurement processing, a powerful hardware signal processor module converts time data to frequency data using the latest FFT technology. The analyzer has a dynamic range of 72 dB and maximum frequency span of 12.8kHz. It can acquire data at a maximum rate of 32,768 samples/sec per channel with a cross channel accuracy of 0.1dB (plus or minus). The most important measurement capabilities provided by the software of the analyzer include: time record, RPM spectral map, auto-correlation, cross-correlation, frequency response gain phase, power spectrum, cross spectrum, histogram, order tracking and order ratio map.

This project processes large amount of test data. A high speed, multichannel data acquisition and processing system is vital to this investigation. In addition, the system should offer flexibility to its users for post-processing of data during data analysis phase. The existing Spectrum and Network Analyzer is not designed for mass reduction and analysis of data. As a result, data processing by the existing system is basically manual, through a menu driven environment. It is extremely time consuming and labor intensive. For example, one data point (about 30 seconds recorded data) will take 2 to 3 weeks to process. Therefore, to speed up the data processing it is necessary to develop a new system which will acquire and analyze the data in a more efficient way.

Clark Atlanta University purchased the hardware and software for the development of the new data acquisition and analysis system. The system consists of a Intel 80486 DX 66MHz based computer, data acquisition boards and necessary software. The system is a high speed multichannel data acquisition and processing system, which consists of a based computer equipped with IEEE488 interface. It uses two data acquisition boards. The first one is a National Instrument EISA-A2000 High Performance Data Acquisition board which is a 12 bit resolution A/D plug-in board for the EISA bus with a 1 MHz sampling rate. The board has four analog input channels, each with its own track-and-hold(T/H) circuitry. It can be used in laboratory and industrial environments for instrumentation, waveform recording, and electronic test and measurement applications. The fast 12 bit resolution analog input makes the board useful for high performance signal analysis, transient

analysis, pulse-parameter measurement, and data logging. The second data acquisition board is National Instrument AT-MIO-16X. The AT-M10-16X is a high resolution, high performance, multifunction analog, digital, and timing I/O board for the PC AT and compatible computers. It contains a 16 bit, 100KHz, sampling ADC with up to 16 analog inputs, two 16 bit DACs with voltage outputs, eight lines of transistor transistor logic (TTL) compatible digital I/O, and three 16 bit counter/timer channels for timing I/O.

The primary software for instrument control and data acquisition is Laboratory Virtual Instrument Engineering Workbench (Lab VIEW) developed by National Instruments Corporation. LabVIEW is a software system for building high-performance instrumentation and analysis applications. It features a unique icon-based graphical compiled programming language and user interface that provide an integrated environment for engineering and scientific applications. Data can be acquired from GPIB, VXI, RS232 instruments or from National Instruments' plug-in data acquisition board. More than 1430 instruments can be controlled by the ready-to-use icons in the Instruments Library. Analysis functions in LabVIEW include statistical processing, array manipulation and digital signal processing. The graphical user interface includes color graphics with special pan and zoom features and picture import capabilities. To share resources and exchange information with other research communities, this system is equipped with Ethernet interface.

Software has been developed under LabVIEW for data processing. The program is used to acquire the data from an external source (the tape drive in our case) and run an FFT operation on the data acquired. The front panel which provides a virtual instrument environment. Through the front panel, the data acquisition board (device), the channels, the amount of data point in each block for FFT, and the sampling frequency can be specified in the front panel. In addition, the windowing function and the low pass filter can be turned on or off, depending upon the needs. The spectrum of the signals will be displayed with the time trace on the front panel. The peak value of the spectrum and the frequency at which the peak is located will also be displayed. Further more, the engine rotor speed, which is converted from the NL signals on the 12th track of the analog data tape, is shown graphically by a meter.

2.2 Reduction of Experimental Data

The reduction procedure of the tape recorded data is as follows:

(a) The tape recorded data are first reproduced by the tape system at the speed at which they were recorded. To ensure the accurate reproduction of the data, the output amplifier of the tape drive is calibrated following the manufacturer's instruction.

(b) The output signals selected from 8 of the 14 output channels of the tape deck are then fed to the input channels of the spectrum analyzer. The signals are digitized and converted.

(c) The signals from the 8 channels are continuously monitored by watching the real time display on the computer's monitor. The data section of interest is then determined.

(d) The selected data section is then acquired into the RAM as a time captured data file.

(e) The time captured data file is then analyzed by using different features of the measurement software and the results plotted.

(f) Step (c) for the following portion of the tape is repeated until all the data recorded on the tape are analyzed.

All the five data tapes which we have received have been analyzed. The results obtained from the analysis include Campbell diagrams and damping identification. In addition, the effects of engine sweeping upon the vibrational response has also been studied. These analysis results will be briefly reviewed in the following.

Campbell Diagrams -- The data obtained from spectrum analysis have been used to construct the Campbell diagrams. These diagrams were constructed by programs developed at CAU, which generates the Campbell diagrams based upon the above mentioned FFT results. The computer code of this program has been reported in previous quarterly reports. The data obtained revealed that all vibrations are forced vibrations which correspond to the 32 order excitations. Examinations of the Campbell diagrams confirm that all significant vibrations are order-related, and they are of the order 32, which is exactly the number of blades on the first stage of the fan. The first stage fan is located immediately down stream of the front frame struts. So far, all the results from various struts conclusively indicate that the excessive vibration of the front frame struts are caused by the downstream flow disturbance that is induced by the sweeping of the first stage fan of the compressor. Since the fan is at the downstream, this disturbance must have been propagated acoustically and

exerted on the front frame struts. Therefore, the modeling of the fluid flow and acoustic field in the engine duct and investigation of the interaction among the acoustic waves, fluid flow and the strut structure are critical to the elucidation of the physical causes of the excessive vibrations.

Damping Identification -- This work is motivated by efforts to understand the causes of excessive vibration stresses which have resulted in premature failures of the front frame struts of the engine. In order to isolate the trends in the occurrence of these unusually high stresses, it is necessary to obtain estimates of the effective damping of the structure at different engine operating conditions. The conventional processing of engine aeromechanical data e.g., Campbell diagrams etc., do not provide this information. However, it is evident that the forced response data measured while the engine is undergoing aeromechanical testing, may contain sufficient information to estimate the effective damping of the resonant modes. A study of the trends in these damping factors should reveal the possible conditions under which the struts can be expected to experience increased vibrational stresses. Under certain assumptions which appear valid for the operation of jet engines, the techniques which have previously been used to identify modal damping from measurements of structural transfer functions can be applied to estimate the effective damping from the forced response measurements. The key idea is to recognize that although the measured responses themselves are not transfer functions, if the spectra of the excitation forces are nearly uniform, the nature of the forced response spectra in the complex plane, is very similar to that of transfer functions. This requirement is met by the fact that the forced responses of the engine stationary components are derived from engine order excitations whose spectra vary with the engine rotor speed. Therefore, as the rotor speed is steadily increased from low to high, the effective excitation of the engine components are similar to that of a swept sine excitation in modal testing. In the complex plots of the linear forced response spectra, the role of modal constant is played by an unknown quantity (which combines the modal constant and the unknown excitation) which needs not be determined in order to extract the modal damping factor.

The analysis of frequency response data to obtain modal properties was first developed by Kennedy and Pancu (1947) in their work on aircraft flutter testing. Advances made in this field in recent years have been due to the ready availability

of powerful computational resources for the rapid analysis of Fast Fourier Transform. The detailed theory of modal testing and analysis have been presented in several publications i.e.,. [Lang, 1975], [Brown et al, 1977], [Ewins, 1984], [Flannelly et al, 1981], and [Fabunmi et al, 1977]. By starting with the forced responses in the frequency domain, expressed in terms of the mobility functions and the excitation forces, the equations which have previously been used to analyze frequency response functions, can be applied to the linear spectra of the forced responses themselves, in order to yield the modal damping factors. As a result, equations which can be used to develop algorithms for reducing forced response data from engine aeromechanical tests, have been derived. A computer program has also been developed to implement the algorithms.

The linear spectra of the forced responses of a damped structure can be related to the spectra of the excitation forces via the frequency response functions:

$$\{y(\omega)\} = [Y(\omega)]\{f(\omega)\} \tag{1}$$

where {y(w)} is the N x 1 vector of the forced response, {f(w)} is the M x 1 vector of the excitation forces, and [Y(w)] is the N x M matrix of the structural frequency response functions. In other words, the response spectra at coordinate "i" due to forces at all the M excitation coordinates is given by:

$$y_i(\omega) = \sum_{j=1}^{M} Y_{ij}(\omega) f_j(\omega) \tag{2}$$

For a fairly general class of damping mechanisms, the expression for the matrix [Y(w)] has been shown to be [Fabunmi, 1985]:

$$\{Y(\omega)\} = \sum_{n=1}^{N\to\infty} \left[\frac{\{\phi\}_n \{\phi\}_n^T}{m_n}\right] \frac{1}{\Omega_n^2 (1 - (\omega^2/\Omega_n^2) + i g_n(\omega))} \tag{3}$$

where $\{\phi\}_n$ is the n-th orthonormal mode vector of the structure, $\{\phi\}_n^T$ is its transpose, m_n is the n-th modal mass, Ω_n is the frequency of the n-th mode, and $g_n(\omega)$ is the frequency dependent damping coefficient of the n-th mode. If the element (i, j) of the matrix $\left[\frac{\{\phi\}_n \{\phi\}_n^T}{m_n}\right]$ is demoted by A_{ijn}, then:

$$Y_{ij}(\omega) = \sum_{n=1}^{N\to\infty} \frac{A_{ijn}}{\Omega_n^2 (1 - (\omega^2/\Omega_n^2) + i g_n(\omega))} \tag{4}$$

and the forced response at coordinate i become:

$$y_i(\omega) = \sum_{j=1}^{M} \sum_{n=1}^{N\to\infty} \frac{A_{ijn} f_j(\omega)}{\Omega_n^2 (1 - (\omega^2/\Omega_n^2) + i g_n(\omega))} \tag{5}$$

Further, let:

$$B_{in}(\omega) = \sum_{j=1}^{M} \frac{A_{ijn} f_j(\omega)}{\Omega_n^2} \tag{6}$$

and,

$$G_n(\omega) = \frac{1}{1 - (\omega^2/\Omega_n^2) + i g_n(\omega)} \tag{7}$$

then the forced response at coordinate i can be written as:

$$y_i(\omega) = \sum_{n=1}^{N\to\infty} B_{in}(\omega) G_n(\omega) \tag{8}$$

At frequencies close to the resonance of mode n, the forced response is dominated by the contribution of that made to the series in Eq. 8. In the neighborhood of this frequency, following the assumption that the spectra of the excitation forces does not vary sharply with frequency, the forced response can therefore be approximated by the following expression:

$$y_i(\omega) \approx B_{in}(\omega) G_n(\omega) + \varepsilon_n \qquad (\Omega_n - \Delta < \omega < \Omega_n + \Delta; \quad \Delta \to 0) \tag{9}$$

where ε_n is a complex valued residual due to the contributions of the remaining truncated modes. All the quantities in Eq. 9 are complex valued, and in the neighborhood of the resonant frequency Ω_n, the frequency behavior of $G_n(\omega)$governs the frequency behavior of the forced response. It will further be assumed that the damping function $g_n(\omega)$ appearing in the definition of $G_n(\omega)$ is approximated by its value at $\omega = \Omega_n$, thus:

$$G_n(\omega) \approx \frac{1}{1 - (\omega^2/\Omega_n^2) + i g_n(\omega)} \tag{10}$$

In the subsequent discussions, $g_n(\omega)$ will be referenced simply as g_n, the damping coefficient of the n-th mode. The function represented by Eq. 10 has been

the subject of extensive analysis in publications on the subject modal testing and analysis. The following is a brief review of its more relevant properties. The real and imaginary parts of $G_n(\omega)$ are:

$$\mathrm{Re}(G_n(\omega)) = \frac{1-(\omega^2/\Omega_n^2)}{(1-(\omega^2/\Omega_n^2))^2 + g_n^2} \tag{11}$$

$$\mathrm{Im}(G_n(\omega)) = \frac{-g_n}{(1-(\omega^2/\Omega_n^2))^2 + g_n^2} \tag{12}$$

It follows that:

$$\mathrm{Re}(G_n(\omega))^2 + \mathrm{Im}(G_n(\omega))^2 = -\frac{\mathrm{Im}(G_n(\omega))}{g_n} \tag{13}$$

or,

$$\mathrm{Re}(G_n(\omega))^2 + \left(\mathrm{Im}(G_n(\omega)) + \frac{1}{2g_n}\right)^2 = -\frac{1}{4g_n^2} \tag{14}$$

On a Nyquist plot of $G_n(\omega)$, with $\mathrm{Im}(G_n(\omega)$ as ordinate and $\mathrm{Re}(G_n(\omega))$ as abscissa and frequency as parameter, according to Eq. 14, a circle will be obtained. Its center will be at coordinate $(0, -\frac{1}{2g_n})$, and its radius will be $\frac{1}{2g_n}$. For any pair of points on the circle, lying on opposite sides of the resonant frequency, the damping coefficient can be expressed as follows:

$$g_n = \frac{\omega_+^2 - \omega_-^2}{\Omega_n^2(\tan(\theta_+) + \tan(\theta_-))} \tag{15}$$

From Eq. (9), the arc of the Nyquist plot of the forced response spectra will be part of a circle which has been amplified by a factor of $|B_{in}(\omega)|$, rotated about the origin through an angle of $\arg(B_{in}(\omega))$ and then shifted from the origin by the complex residual ε_n. The circle that is fitted to the data in the neighborhood of the resonant frequency will have an origin at some coordinate (a,b). The point on this circle, diametrically opposite the resonant frequency will have coordinate (e,f). If the forced response data in the neighborhood of the resonant frequency are represented by an ordered set of numbers denoted by:

$$(\omega_i; \mathrm{Re}(y(\omega_i)); \mathrm{Im}(y(\omega_i))); \qquad i = -L, -(L-1), \ldots\ldots -1, 0, 1, \ldots\ldots L-1, L; \quad \omega_0 = \Omega_n;$$

then following are the necessary formulas needed to identify the modal damping from the forced response spectra:

For each data point i that lies on the circle, we must have:

$$\left(\mathrm{Re}(y(\omega_i)) - a\right)^2 + \left(\mathrm{Im}(y(\omega_i)) - b\right)^2 = R^2 \tag{16}$$

which expands to:

$$\mathrm{Re}(y(\omega_i))^2 + \mathrm{Im}(y(\omega_i))^2 - 2a\,\mathrm{Re}\left(y(\omega_i)\right) - 2b\,\mathrm{Im}(y(\omega_i)) = R^2 - a^2 - b^2 \tag{17}$$

For i=0, $\omega_0 = \Omega_n$, we have:

$$\mathrm{Re}(y(\Omega_n))^2 + \mathrm{Im}(y(\Omega_n))^2 - 2a\,\mathrm{Re}\left(y(\Omega_n)\right) - 2b\,\mathrm{Im}(y(\Omega_n)) = R^2 - a^2 - b^2 \tag{18}$$

From above two equations, by subtracting one from another we can have:

$$\begin{aligned}&\left(\mathrm{Re}(y(\omega_i))^2 - \mathrm{Re}(y(\Omega_n))^2\right) + \left(\mathrm{Im}(y(\omega_i))^2 - \mathrm{Im}(y(\Omega_n))^2\right)\\ &= 2a\left(\mathrm{Re}(y(\omega_i)) - \mathrm{Re}(y(\Omega_n))\right) + 2b\left(\mathrm{Im}(y(\omega_i)) - \mathrm{Im}(y(\Omega_n))\right)\end{aligned} \tag{19}$$

Because the actual data points will not lie exactly on the circle, the error is defined as:

$$\begin{aligned}\varepsilon_i = &\left(\mathrm{Re}(y(\omega_i))^2 - \mathrm{Re}(y(\Omega_n))^2\right) + \left(\mathrm{Im}(y(\omega_i))^2 - \mathrm{Im}(y(\Omega_n))^2\right)\\ &- 2a\left(\mathrm{Re}(y(\omega_i)) - \mathrm{Re}(y(\Omega_n))\right) + 2b\left(\mathrm{Im}(y(\omega_i)) - \mathrm{Im}(y(\Omega_n))\right)\end{aligned} \tag{20}$$

To find (a, b) which minimizes the sum of the squared error, we define:

$$s = \sum_i \varepsilon_i^{\,2} \tag{21}$$

For s with respect to (a, b), we require:

$$\frac{\partial s}{\partial a} = \sum_i 2\varepsilon_i \frac{\partial \varepsilon_i}{\partial a} = 0 \tag{22}$$

and ,

$$\frac{\partial s}{\partial b} = \sum_i 2\varepsilon_i \frac{\partial \varepsilon_i}{\partial b} = 0 \tag{23}$$

which gives:

$$\begin{bmatrix} A & C \\ C & B \end{bmatrix} \begin{Bmatrix} a \\ b \end{Bmatrix} = \begin{Bmatrix} E \\ F \end{Bmatrix} \tag{24}$$

where:

$$A = \sum_{i=-L}^{L} 4[\mathrm{Re}(y(\omega_i)) - \mathrm{Re}(y(\Omega_n))]^2 \tag{25}$$

$$B = \sum_{i=-L}^{L} 4[\mathrm{Im}(y(\omega_i)) - \mathrm{Im}(y(\Omega_n))]^2 \tag{26}$$

$$C = \sum_{i=-L}^{L} 4[\mathrm{Re}(y(\omega_i)) - \mathrm{Re}(y(\Omega_n))][\mathrm{Im}(y(\omega_i)) - \mathrm{Im}(y(\Omega_n))] \tag{27}$$

$$E = \sum_{i=-L}^{L} 2[\mathrm{Re}(y(\omega_i)) - \mathrm{Re}(y(\Omega_n))][\{\mathrm{Re}(y(\omega_i))^2 - \mathrm{Re}(y(\Omega_n))^2\} + \{\mathrm{Im}(y(\omega_i))^2 - \mathrm{Im}(y(\Omega_n))^2\}] \tag{28}$$

$$F = \sum_{i=-L}^{L} 2[\mathrm{Im}(y(\omega_i)) - \mathrm{Im}(y(\Omega_n))][\{\mathrm{Re}(y(\omega_i))^2 - \mathrm{Re}(y(\Omega_n))^2\} + \{\mathrm{Im}(y(\omega_i))^2 - \mathrm{Im}(y(\Omega_n))^2\}] \tag{29}$$

so that:

$$a = 2\left(\frac{BE - CF}{AB - C^2}\right) \tag{30}$$

$$b = 2\left(\frac{AF - CE}{AB - C^2}\right) \tag{31}$$

The coordinate (e,f) is:

$$e = 2\left(\frac{BE - CF}{AB - C^2}\right) - \mathrm{Re}(y(\Omega_n)) \tag{32}$$

$$f = 2\left(\frac{AF - CE}{AB - C^2}\right) - \mathrm{Im}(y(\Omega_n)) \tag{33}$$

Now, the modal damping coefficient can be calculated as follows:

$$g_n^{i,j} = \frac{\omega_{+i}^2 - \omega_{-i}^2}{\Omega_n^2(\tan(\theta_{+i}) + \tan(\theta_{-i}))} \tag{34}$$

where:

$$\theta_{+i} = \arccos \frac{[\mathrm{Re}(y(\omega_{+i})) - e][\mathrm{Re}(y(\Omega_n)) - e] + [\mathrm{Im}(y(\omega_{+i})) - f][\mathrm{Im}(y(\Omega_n)) - f]}{\sqrt{\{[\mathrm{Re}(y(\omega_{+i})) - e]^2 + [\mathrm{Im}(y(\omega_{+i})) - f]^2\}\{[\mathrm{Re}(y(\Omega_n)) - e]^2 + [\mathrm{Im}(y(\Omega_n)) - f]^2\}}} \quad (35)$$

$$\theta_{-i} = \arccos \frac{[\mathrm{Re}(y(\omega_{-i})) - e][\mathrm{Re}(y(\Omega_n)) - e] + [\mathrm{Im}(y(\omega_{-i})) - f][\mathrm{Im}(y(\Omega_n)) - f]}{\sqrt{\{[\mathrm{Re}(y(\omega_{-i})) - e]^2 + [\mathrm{Im}(y(\omega_{-i})) - f]^2\}\{[\mathrm{Re}(y(\Omega_n)) - e]^2 + [\mathrm{Im}(y(\Omega_n)) - f]^2\}}} \quad (36)$$

The superscript "i,j" in Eq. 16 has been used to underscore the fact that due to the imperfection of measured data, and the approximate nature of the circle fit technique, the value of the damping coefficient calculated using different pairs of points on either side of the resonant frequency, will differ slightly from each other. If all possible combinations of i,j are used, then a statistical technique can be used to determine the mean value of the damping coefficient, as well as its standard deviation.

The software package that came with the Multi-channel Spectrum/Network Analyzer--HP 3566A does not provide the feature to conduct the curve fitting. In addition, the raw data and the results from the FFT routine of the software package are stored in the SDF format. Therefore, to use the data acquired by the HP analyzer and the measurement results from the provided software, the data must be converted into ASCII format so that computer programs written in languages such as Quick Basic, FORTRAN and/or C can be used to further analyze the data. After careful examination of the SDF format and the data storage structure used in the provided software, utility softwares have been used to convert the needed data into ASCII format and then a program has been used to re-arrange the data into a multi-column structure which is convenient to future analysis. Then, a program which conducts circle fitting and calculates the modal damping coefficient is developed. The algorithm and the developed software have been used on the available data tapes to obtain some preliminary results. However, since a complete damping coefficient survey would require data recorded under different engine operating conditions and these additional data tapes have not been made available to CAU, only limited preliminary damping coefficient results are obtained and reported.

The Effects of Engine Sweeping -- Since the signals were recorded when the engine was decelerating and accelerating respectively, it provides an opportunity to compare the Campbell diagrams for the same pressure probe or strain gauge to investigate the effect of the engine acceleration or deceleration on the vibratory response of the front frame struts. Comparison of the Campbell diagram for the

same pressure probe or strain gauge concludes that the measurement conducted in the deceleration and acceleration process produce same resonant frequencies, roughly the same amplitude of the resonance, and the similar overall trend of the response as the engine speed changes. However, these figures also indicate that although all of them show similar resonant peaks at the same frequencies, the magnitudes of the second peak at the higher frequency are different. It appears that when the engine was accelerating, the response is the highest, and the higher deceleration rate produced the lowest response level.

2.3 Computational Resources

Computational resources - hardware and software- required to perform numerical analysis of unsteady viscous flows through axial flow compressors/turbines depends largely on the level of approximations used. For two-dimensional analysis, current generation UNIX workstations give acceptable performance. A computer code (STAGE-2) developed at NASA Ames to perform 2-D viscous flow analysis through the rotor-stator combination was identified as a suitable candidate because a version of STAGE-2 existed which gave acceptable performance on UNIX workstation. Post processing software such as PLOT3D and FAST were also purchased. Also, a comparison of available workstations was done and Silicon Graphic Indigo with Elan Graphics option was purchased. This workstation had 64 MB of memory and 1 GB of disk space. Later, Clark Atlanta University also acquired an IBM Power Parallel system SP1 with 8 nodes and was used for flow analysis.

2.4 Modeling of the Fluid Flow in Front Frame/Fan Region

Unsteady flow analysis through a rotor-stator combination such as the IGV/rotor from first stage fan is complex and time consuming even for a 2-D case. In order to calculate time accurate flows, it was decided to do 2-D unsteady viscous flow analysis at several appropriate radial locations along the Front frame struts/rotor of the first stage of fan. This would provide time-accurate pressure distribution at specified operating conditions and result in an envelope of aerodynamic loading on the front frame strut which will then be used in the forced response analysis. With this in mind, hardware/software combination described above were acquired.

2.4.1 Calibration of the Code

STAGE-2 code obtained from NASA Ames was installed on Silicon Graphics Indigo, Elan Graphics Workstation. First step in using this code was to check if this code has been installed correctly. This was done by compiling this code and running it on a sample geometry provided with the code. Results obtained for first five time steps were compared with the results in a sample output provided with the code. This test case validated the installation of the code.

Next logical step was to run this code for a well known test case and see if this code reproduces results reported in published literature. This would also provide much needed practice and insight in using this code. Details of a test case and results obtained from it are described below.

2.4.1.1. Description of Test Case:

Flow inside a two-stage axial-flow compressor with inlet guide vanes has been studied in aerodynamic tests at a low Mach number (Test Case E/CO-5 in AGARD Advisory Report No. 275). The inlet flow is drawn from ambient air and the flow field throughout out the facility is essentially incompressible, (relative Mach number being less than 0.14). The two-stage compressor model has a 5 ft. tip diameter and a hub/tip ratio of 0.8. The mid span wheel speed (at r/R=0.9) is U_m = 153 ft/sec and the nominal design flow coefficient is C_X/U_m = 0.51 where C_X is the average axial flow velocity. The flow path consists of a row of inlet guide vane (IGV) followed by two similar stages: Rotor 1, Stator 1, Rotor 2, Stator 2. The only difference between the stages is that the Rotor 1 stagger angle is increased by 3 degrees relative to the Rotor 2 stagger angle. There are 44 airfoils in the IGV and both stators and rotors.

2.4.1.2. Grid System

All blade geometries are defined by NACA 65 - series sections with circular arc mean camber lines. The geometry files was provided by Gundy-Burlet (NASA Ames Research Center) with permission from Robert P. Dring (United Technologies Research Center). Since there are 44 airfoils in each row, it was assumed that the flow is periodic from airfoil to airfoil in the circumferential direction, so the flow through only one airfoil-to- airfoil passage needs to be computed.

STAGE-2 code developed at NASA Ames by Gundy-Burlet and Rai (1987, 1988, 1989, 1991) is meant to be very flexible in accepting axial flow geometries with differing number of stages and airfoils in each row. A simple bookkeeping system

exists which allows this flexibility. The grid system essentially consists of a system of patched and overlaid grids. If 'n' is the number of rows in the axial direction, then 2 x $(n+1)$ types of zones are used to discretize the flow field. The first and last zones are the inlet and outlet zones respectively. Each airfoil has an inner "O" grid and an overlapping outer grid. The inner and outer zones associated with the N^{th} airfoil are $(2xN)^{th}$ and $(2xN+1)^{th}$ zones respectively. Using this system, 12 grids are required to discretize the five-row system of the compressor. The grid and numbering system are as follows. The inner "O" grids (zones 2, 4, 6, 8, and 10) are generated by an elliptic grid generation process. The grid is densely packed close to surface to resolve viscous effects adequately. The grid size in inner "O" grid is 131 X 25. The grid size at inlet zone (zone 1) and exit zone (zone 12) are 28 X 51 each. The outer grids (zones 3, 5, 7, 9 and 11) are 80 X 51 each and are algebraically generated by shearing Cartesian meshes. Thus the total number of grid points in all 12 zones are 39,631.

2.4.1.3 Boundary Conditions:

There are natural boundary conditions at the compressor inlet and exit as well as the airfoil surfaces. In addition, there are zonal boundary conditions because different zones are used to compute the flow at regions where viscous effects predominate (inner zones) and are important and far away from airfoils where viscous effects are not important (outer zones). These zones overlap at inner and outer zone boundaries and are explained in sufficient details in published works of Rai and Gundy-Burlet (1987, 1988, 1989, 1991). Data are transferred from the outer grid to the inner grid along the inner grid's outermost grid line. Information is then transferred back to the outer grid along its inner boundary. This is done using a nonconservative, linear interpolation technique. Stability is improved by increasing the overlap area. The patch boundaries are also treated in a nonconservative manner. Linear interpolation is used to reach over into the adjoining grid to integrate through the patch boundary.

The conditions throughout the compressor are subsonic. According to characteristic theory, three quantities are specified at the inlet, while one quantity is extrapolated from the interior of the compressor. The flow angle, upstream Riemann invariant, and average total pressure are specified while the downstream Riemann invariant is extrapolated from the interior of the inlet. At the exit, three quantities are extrapolated from the interior and one is specified. The average static pressure is specified, while the upstream Riemann invariant, circumferential

velocity, and entropy are extrapolated from the interior. The exit static pressure is specified to be equal to the experimentally determined exit pressure.

The inner boundaries of the body-fitting "O" grids coincide with the airfoil surfaces. Adiabatic-wall, zero-normal-pressure-gradient, and no-slip boundary conditions are imposed on these body surfaces. In the case of the IGV and both stators, the no-slip condition implies specification of zero velocity. For the rotors, the no-slip condition requires that the fluid velocity vector of the surface be set equal to the rotor translation velocity vector. These boundary conditions are implemented implicitly within the iterative integration scheme. Additional details regarding both zonal and natural boundary condition can be found in Rai (1987).

2.4.1.4 Results:

Results were presented for the 2-1/2 stage compressor geometry in the quarterly report dated April 23, 1993. Three iterations were performed at each time step, resulting in drop in residual. In the following discussion, a 'cycle' is defined as motion of the blade through an angle equal to $\frac{2\pi}{N}$, where N is the number of blades in stator airfoil following the rotor. Initially, computations were started with a relatively smaller time step (5000 time steps per cycle), and it was gradually increased to 500 time steps per cycle.

2.4.2 Computations for IGV/Rotor of First Stage of Fan:

In order to initiate flow analysis in the front frame area of the engine under consideration, geometric data and flow conditions are needed. These were requested but only incomplete information was received about geometry and no flow condition data were provided. Thus the geometry and flow conditions were assumed to initiate computations. There are 13 struts/flaps and 32 rotor blades in the first stage of fan. To do the flow analysis, we chose to compute flow on 2 struts/flaps and 5 rotor sections. In the circumferential direction, we distributed seven such combinations, which meant flow simulation for a geometry of 14 strut/flaps and 35 rotor blades. To account for this and to keep the same blockage ratio, geometry had to be modified by factors of 13/14 for strut/flap and 32/35 for rotor in the circumferential direction. A grid was generated for such a combination. There are a total of 21 subgrids and grid sizes for each of these sub grids are shown below:

Grid	Size	No. of grids
Inlet grid for each strut/flap	35X76	2
Inner grid for each strut/flap	161X51	2
Outer grid for each strut/flap	81X76	2
Inner grid for each rotor	121X51	5
Outer grid for each rotor	60X31	5
Outlet grid for each rotor	35X31	5

Total number of grid points for the 2 strut/flap- 5 rotor combination: 84,954.

Using the grid information generated from this data, flow analysis required specification of other operational data about the engine. Without having access to any such information, following was assumed:

Inlet temperature:	540°R
Freestream Mach number:	0.35
Initial flow coefficient:	0.58
Ratio of exit static pressure to inlet total pressure	1.015
Reynolds Number per inch	160,000

With the initial flow coefficient having a value of 0.58, rotor speed is 0.714.

Using this information computations were started using the flow solver component of STAGE-2. Computations were initiated using a low value of Courant Number of 10 and 5000 time steps per cycle. Here a cycle is defined as the travel of all five rotors past the 2 strut/flap combination. Soon it was discovered that time steps per cycles needs to be increased to have stable solution. It was raised from 5000 to 10000 and then reduced progressively to avoid blowing the solution, and finally the solution stabilized at 7000 time steps per cycle. This computation thus is very time consuming and were performed on a single node of IBM SP1. Computational results were reported in quarterly reports dated July 20, 1994 through July 24, 1995.

2.5 Student Training and Education

This project initiated and implemented a rigorous program of undergraduate and graduate student involvement in the project. These students were introduced to mathematical and mechanical vibration concepts so that they could understand the data reduction process. Appendix A includes the report which provides details about their participation and progress.

2.6 Reports, Presentations, and Publications

During the period of the project, following reports, presentations, and publications have been generated, in addition to monthly reports:

Reports:

Item No	Report Type	Covering Period	Date Delivered
01	Annual Report	January 1 - December 31, 1991	January 6, 1992
02	Annual Report (Revised)	January 1 - December 31, 1991	March, 1992
03	Quarterly Report	January 1 - March 31, 1992	April 9, 1992
04	Quarterly Report	April 1 - June 30, 1992	July 15, 1992
05	Quarterly Report	July 1 - September 30, 1992	October 20, 1992
06	Quarterly Report	October 1 - December 31, 1992	January 20, 1993
07	Annual Report	January 1 - December 31, 1992	January 12, 1993
08	Quarterly Report	January 1 - March 31, 1993	April 23, 1993
09	Quarterly Report	April 1 - June 30, 1993	July 21, 1993
10	Quarterly Report	July 1 - September 30, 1993	October 21, 1993
11	Quarterly Report	October 1 - December 31, 1993	January 21, 1994
12	Annual Report	January 1 - December 31, 1993	January 24, 1994
13	Quarterly Report	January 1 - March 31, 1994	April 25, 1994
14	Quarterly Report	April 1 - June 30, 1994	July 20, 1994
15	Quarterly Report	July 1 - September 30, 1994	October 25, 1994
16	Quarterly Report	October 1 - December 31, 1994	January 24, 1995
17	Annual Report	January 1 - December 31, 1994	January 24, 1995

Item No	Report Type	Covering Period	Date Delivered
18	Quarterly Report	January 1 - March 31, 1995	April 24, 1995
19	Quarterly Report	April 1 - June 30, 1995	July 24, 1995
20	Final Report	September 20, 1990 - September 19, 1995	November 15, 1995

Presentations:

01	Project Briefing	Place - Wright Labs	April 15, 1992
02	Project Briefing	Place - Atlanta, GA	November 17, 1992
03	Presentation	Place - Orlando, FL	February 1993
04	Project Briefing	Place - Atlanta, GA	August 30, 1993

Publications:

Fabunmi, J. A., Bai, T., Puri, O., Bota, K., and Sunderland, Lt. Carolyn, "Aero-Engine Component Damping Estimation From Full-Scale Aeromechanical Test Data," AIAA Paper 93-1873, AIAA/SAE/ASME/ASEE 29th Joint Propulsion Conference and Exhibit, June 28-30, 1993, Monterey, CA.

Ferguson, F., Fabunmi, J. A., and Bai, T., "An Analysis of Aeroelastic Response of Vibrating Surfaces," AIAA Paper 95-0724, 33rd AIAA Aerospace Sciences Meeting and Exhibit, January 9-12, 1995, Reno, NV.

Echols, C., Silimon, D., Singh, J., and Bai, T., "Application of FFT on Aero-Engine Data Analysis", Second Annual HBCU/Private Sector Energy Research and Development Technology Transfer Symposium, 1994.

3. CONCLUSIONS

1. We successfully developed aircraft engine aeromechanical test data processing capabilities at Clark Atlanta University.

2. We successfully developed algorithms to identify damping coefficients from full scale engine test data. The algorithms have been implemented in computer code and results are obtained from available data tapes.

3. We successfully processed and analyzed data tapes provided to us under this project. More data tapes covering different operating conditions would have resulted in complete understanding of damping trends.

4. We were successful in acquiring and installing a fluid flow analysis software on a SGI workstation. This software was calibrated and then used to do unsteady viscous flow analysis for assumed geometry data and flow conditions for the front frame/rotor of the engine under consideration. Since requested information about geometry and flow conditions were not provided, a realistic analysis of the unsteady flow could not be carried out to provide any meaningful input for forced response analysis.

5. We were successful in implementing an education and training program for undergraduate engineering and graduate computer science students. They participated in data reduction activities and did publish a paper.

4. REFERENCES

Brown, D., Carbon, G. and Ramsey, K. 1977. "Survey of Excitation Techniques Applicable to the Testing of Automotive Structures," Proceedings SAE, No. 770029.

Capace, V.R. and Fleeter, S. 1987. Unsteady aerodynamic interactions in a multi-stage compressor. *Journal of Tubomachinery*, Transactions of the ASME, Vol. 109, No.3, pp.420-428.

Chi, R.M. 1980. Unsteady aerodynamics in stalled cascade and stall flutter prediction. ASME Paper No. 80-C2/Aero-1.

Ewins, D.J. 1984. "Modal Testing: Theory and Practice," Research Studies Press.

Fabunmi, J.A. 1985. "Extended Damping Models for Vibration Data Analysis," Journal of Sound and Vibration (1985) 101(2), pp. 181-192.

Fabunmi, J.A. and Tasker, F.A. 1988. "Advanced Techniques for Measuring Structural Mobilities," Proc. ASME Journal of Vibration, Acoustics, Stress, and Reliabilities in Design, Vol. 110, pp. 345-349.

Flannelly, W.G., Nagy, E.J. and Fabunmi, J.A. 1981. "Analytical Testing," NASA CR 4329, May 1981.

Giles, M.B. 1990. Stator-rotor interaction in a transonic turbine. *Journal of Propulsion and Power*, Transactions of the ASME, Vol.6, No.5, pp. 621-627.

Gundy-Burlet, K. L., Rai, M. M., and Dring, R. P., "Two-Dimensional Computations of Multi-stage Compressor Flows Using a Zonal Approach," AIAA Paper No. 89-2452

Gundy-Burlet, K. L., Rai, M. M., Stauter, R. C., and Dring, R. P., "Temporally and Spatially Resolved Flows in a Two-Stage Axial Compressor: Part 2 - Computational Assessment," Transactions of the ASME, Journal of Turbomachinery, April 1991, Vol. 113, pp. 227-232.

Gundy-Burlet, K. L., "Computations of Unsteady Multistage Compressor Flows in a Workstation Environment," ASME Paper 91-GT-336, 1991.

Kaji, S. and Okazaki, T. 1970. Generation of sound by rotor-stator interactions. *Journal of Sound and Vibration*, Vol. 13, No. 3, pp 281-307.

Kennedy, C.C. and Pancu, C.D.P. 1947. "Use of Vectors in Vibration Measurement and Analysis," Journal of the Aeronautical Sciences, Vol. 14, No. 11, Nov. 1947.

Kerrebrock, J.L. 1977 Aircraft Engines and Gas Turbines. The MIT Press.

Lang, G.F. 1975. "Understanding Vibration Measurements," Application Note No. 9, Nicolet Scientific Corporation.

Morfey, C.L. 1964. Rotating pressure patterns in ducts: Their generation and transmission, *Journal of Sound and Vibration*, (1964) 1, 60-87.

Namba, M. 1977. Three dimensional analysis of blade force and sound generation for annular cascade in distorted flows. *Journal of Sound and Vibration*, (1977) 50(4), 479-508.

Namba, M. and Ishikawa, A. 1983. Three dimensional aerodynamic characteristics of oscillating supersonic and transonic annular cascades. *Journal of of Engineering for Power* Transactions of the ASME, Vol.105, pp. 138-146.

Oates, G. C., Aerothermodynamics of Gas Turbine and Rocket Propulsion, AIAA Education Series, Washington, DC, 1988

Smith, S.N. 1971. Discrete frequency sound generation in axial flow turbomachines. R&M 3709. Cambridge university, England.

Tyler, J.M. and Caspar, J.R. 1981. Development of a linear unsteady aerodynamic analysis for finite-deflection subsonic cascades. AIAA Paper No. 81-1290R.

Wright, S.E. 1976. The acoustic spectrum of axial flow machines. *Journal of Sound and Vibration*, (1976) 45(2), 165-223.

Rai, M. M., "Navier-Stokes Simulations for Rotor/Stator Interactions Using Patched and Overlaid Grids," J. Propulsion Power, Vol. 3, No. 5, Sept. 1987, pp. 387-396.

Rai, M. M., and Madavan, N. K., "Multi-airfoil Navier-Stokes Simulations of Turbine Rotor-Stator Interaction," AIAA Paper No. 88-0361, 1988.

Clark Atlanta University, AEDAR Corporation, "Research in Structural Dynamics and Control and Aeropropulsion," Quarterly Reports for USAF/WL Contract No. F33615-90-C-2082.

APPENDICES

A. Student Training in "Research in Structural Dynamics and Control and Aeropropulsion," Final Report for September 1992- May 1993.

B. Copy of AIAA Paper 93-1873.

C. Copy of AIAA Paper 95-0724.

Appendix A

Student Training in "Research in Structural Dynamics and Control and Aeropropulsion," Final Report for September 1992- May 1993.

Student Training in "Research in Structural Dynamics and Control and Aeropropulsion"

Final Report for September 1992- May 1993

A. Summary:

Because of the multidisciplinary nature of the project dealing with "Research in Structural Dynamics and Control and Aeropropulsion", three mentors were involved in various phases of this year's training effort (1992-93). These were,

Dr. J. Singh , Ph.D. in Aerospace Engineering,
Dr. N. Talukder, Ph.D. in Mechanical Engineering, and
Dr. T. Bai, Ph.D. in Aerospace Engineering.

Four students were assigned to this project and an assessment was made of their capabilities to participate in research. After this assessment, it was decided that they will have be instructed in fundamentals of applied mathematics and mechanical vibrations before starting with data reduction and analysis. This training was started in September. Dr. Singh instructed in basics of advanced mathematics and that was followed by fundamentals of mechanical vibrations by Dr. Talukder. Dr. Bai, then took over and introduced them to the analysis of experimental data using spectrum analyzer and other data reduction techniques using different computational algorithms. Students have successfully completed this phase.

B. Research Project - An Overview:

This project is titled "Research in Structural Dynamics and Control and Aeropropulsion" and is funded by the Air Force under Contract Number F33615-90-C-2082. It is an ongoing project for the last two years. This presented a unique opportunity for undergraduate students to participate in the research.

The objectives of this research project are to reduce and analyze aeromechanical test data obtained from full scale engine tests at AEDC (Arnold Engineering Development Center), to investigate the causes for excessive vibration response of the front frame struts of the F110-GE-129 high performance turbofan engine, and to develop analytical and/or empirical models for predicting the conditions under which such high responses occur.

Forced response problems in high performance aircraft engines have remained major obstacles which must be overcome. Over the past several decades, considerable research effort has been devoted to the forced response and fluid-

structural instabilities of rotating components such as fan, compressor and turbine rotor systems. The non-rotating components such as stators and the engine front frame have been validated mainly on the bases of their structural stability and integrity without much consideration for fluid-structural interactions.

The excessive stress levels in the front frame of the F110-GE-129 are due to interactions between the strut's structure and the acoustic field in the duct. Although measures have been taken which increase the structural damping of these components, the physical mechanisms responsible for this problem is yet to be established. By inverse reasoning, if the fix to the problem is to apply damping treatments to the components, then whatever is happening during engine operation must be having the effect of reducing the effective damping of the structure. Reasoning along these lines, it must be of interest to investigate how the effective damping of the engine front frame varies with engine operating conditions. Our approach to this investigation is to begin by formulating ways of identifying the effective damping of the front frame struts at different operating conditions. We expect to be able to observe trends in the damping of the engine components at different engine operating conditions. Next, we will attempt to predict those trends by conducting analysis of the fluid-structure interactions in the engine duct.

Initial efforts under this program were concerned with the setup of the necessary data processing and analysis equipment. The data processing equipment has been set up. The system consists of a Multi-channel, Spectrum/Network Analyzer-HP3566A, a 386sx computer system with laser printer, a Macintosh IIsi computer with laser printer, an HONEYWELL Data Storage Model 101e Portable Tape System and software that are necessary to conduct data acquisition, data analysis, results presentation and documentation. This setup is shown in Figure 1. Essentially, the data reduction process produces Campbell diagrams for all the struts that were instrumented with strain gauges. Using these Campbell diagrams, we can identify the type of the vibration, the excitation source, the resonant frequencies, and the magnitude of the maximum stress experienced by the struts.

C. Sample Results:

The experimental data is obtained on magnetic tapes and is read using the Honeywell Portable Tape System. First of all, the time traces from these strain gauges were observed and examined after the signals were digitized and downloaded into the computer. This process helped to determine the sections of the signals that are needed to be analyzed in detail. Then Fast Fourier Transform (FFT) were performed for a small time interval in the selected sections, typically 0.25 seconds. By this operation, the linear spectrum of the

signals at different strain gauges were obtained. From these spectra, the dominating frequency and the amplitude of the oscillating signals were obtained, which were converted into the dynamic stress amplitude by multiplying the calibration factor.

The spectrum analysis is then conducted, one small time interval at a time, for the whole selected section, which may consists of hundreds of small time intervals to be analyzed. The data obtained from the spectrum analysis are, in turn, used to construct the Campbell diagrams, which are shown in Figures 2 and 3 for different struts of the front frame and at locations where strain gauges are mounted. These diagrams were constructed using the computer programs developed at CAU, which generates the Campbell diagrams based upon the above mentioned FFT results. Similar diagrams were generated by students participating in the project.

Other part of this ongoing research project is research on the unsteady fluid flow simulations in the front frame. This is an advanced topic and beyond the scope of undergraduate students having no background in higher mathematics beyond calculus and aerodynamics. Therefore, this aspect of the research was deferred till students participating in the research had adequate background in mathematics and physics to understand advanced unsteady aerodynamic concepts.

D. Conclusions:

Students participating in the WL Research Project had a chance to work on a research topic that is the focus of research at national level. They were able to concentrate on data reduction part of this project. They have gained insights into the usage of personal computers to do data reduction, analysis, and report writing along with some understanding of the multi-disciplinary nature of the project. We believe that this research experience provided them with an opportunity to participate in research outside of classroom settings and reinforce what they had learned through formal classroom lectures. This experience is expected to stimulate their interest to go beyond their undergraduate studies leading to graduate work in a major research institution.

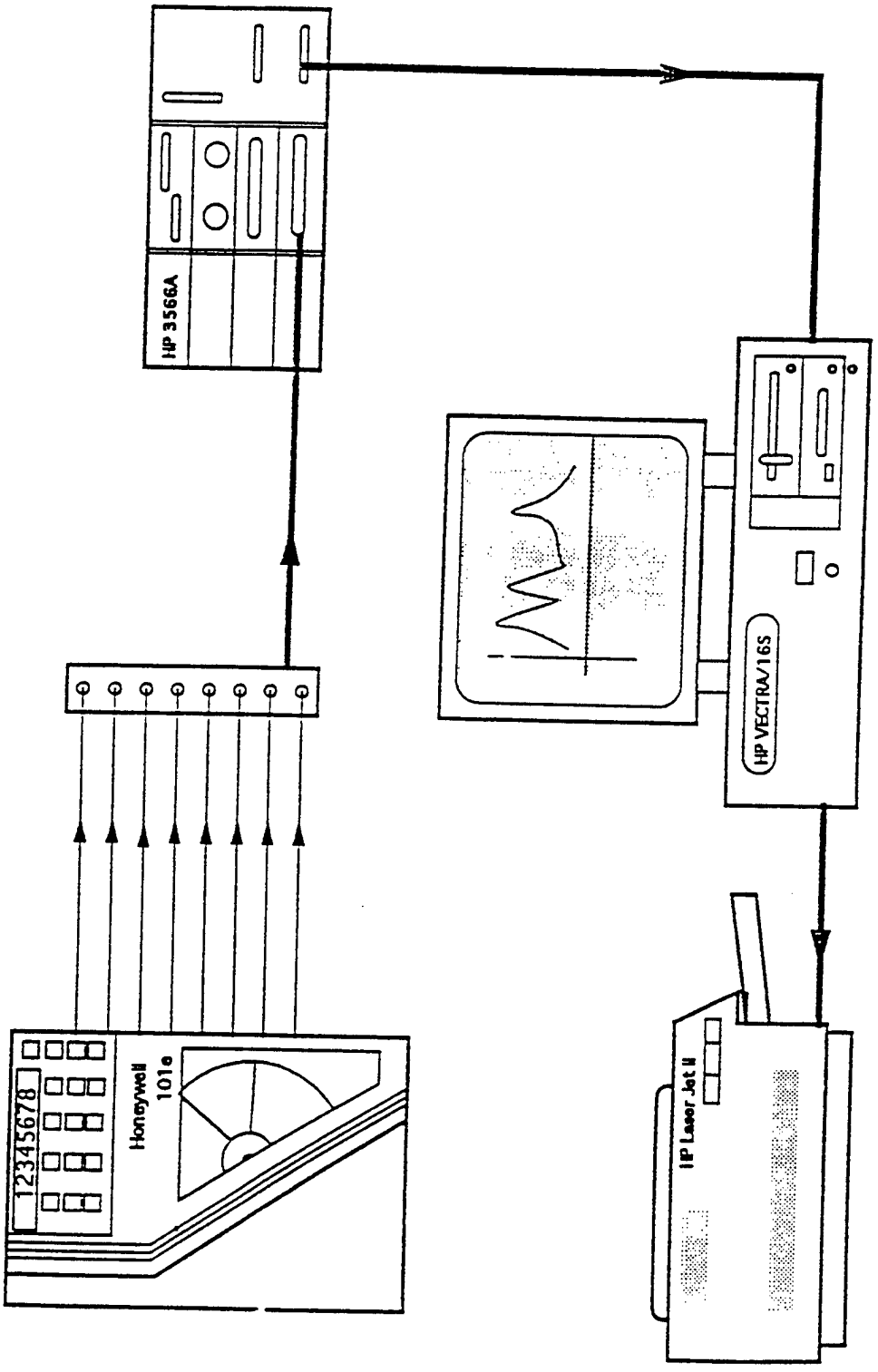

Figure 1. A schematic of the Multi-Channel, Spectrum/Network Analyzer and the tape record/reproduce system.

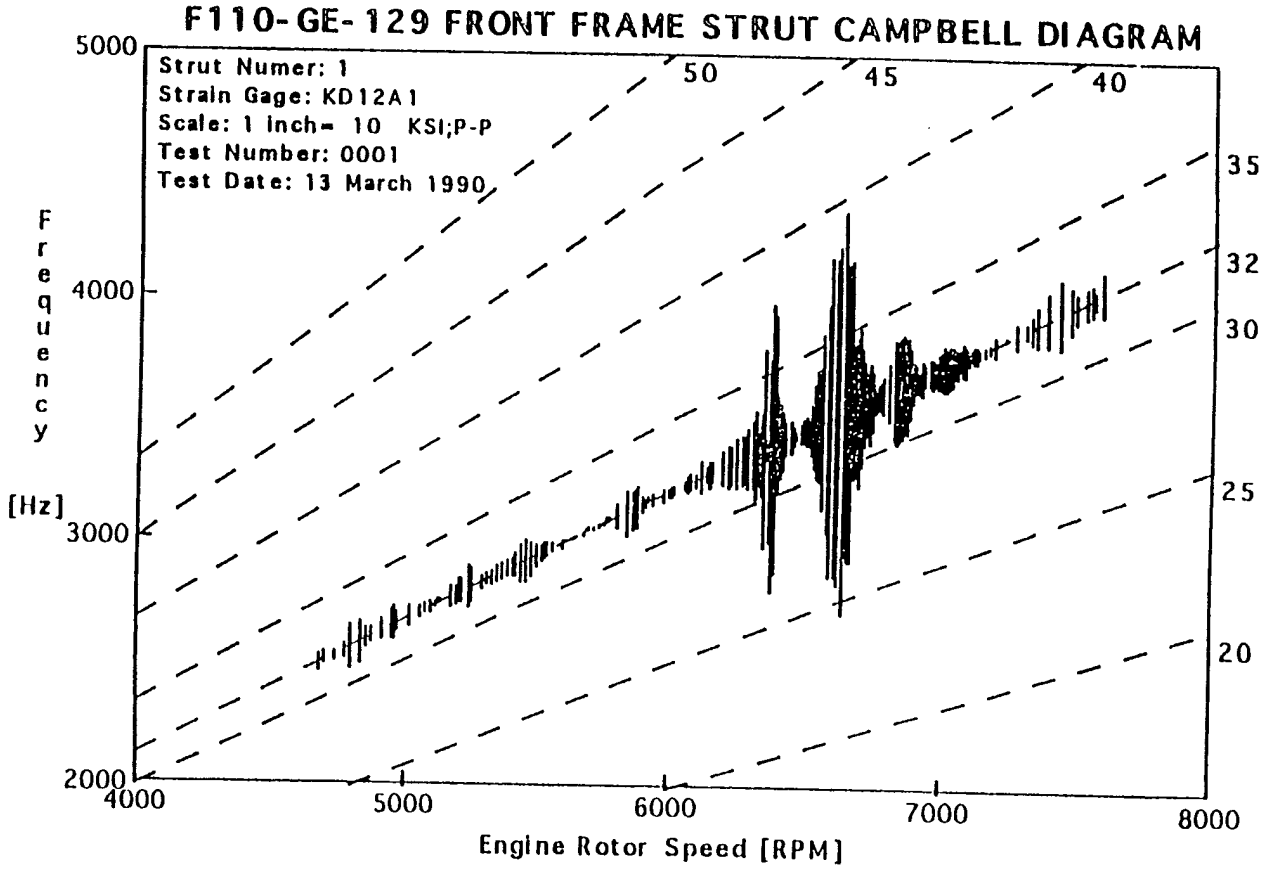

Figure 2. Campbell diagram for KD12A1. Engine working condition: P_1=24 psia, T_1=60 °F. IRIG time: 072:10:15:47 -- 072:10:18:49.

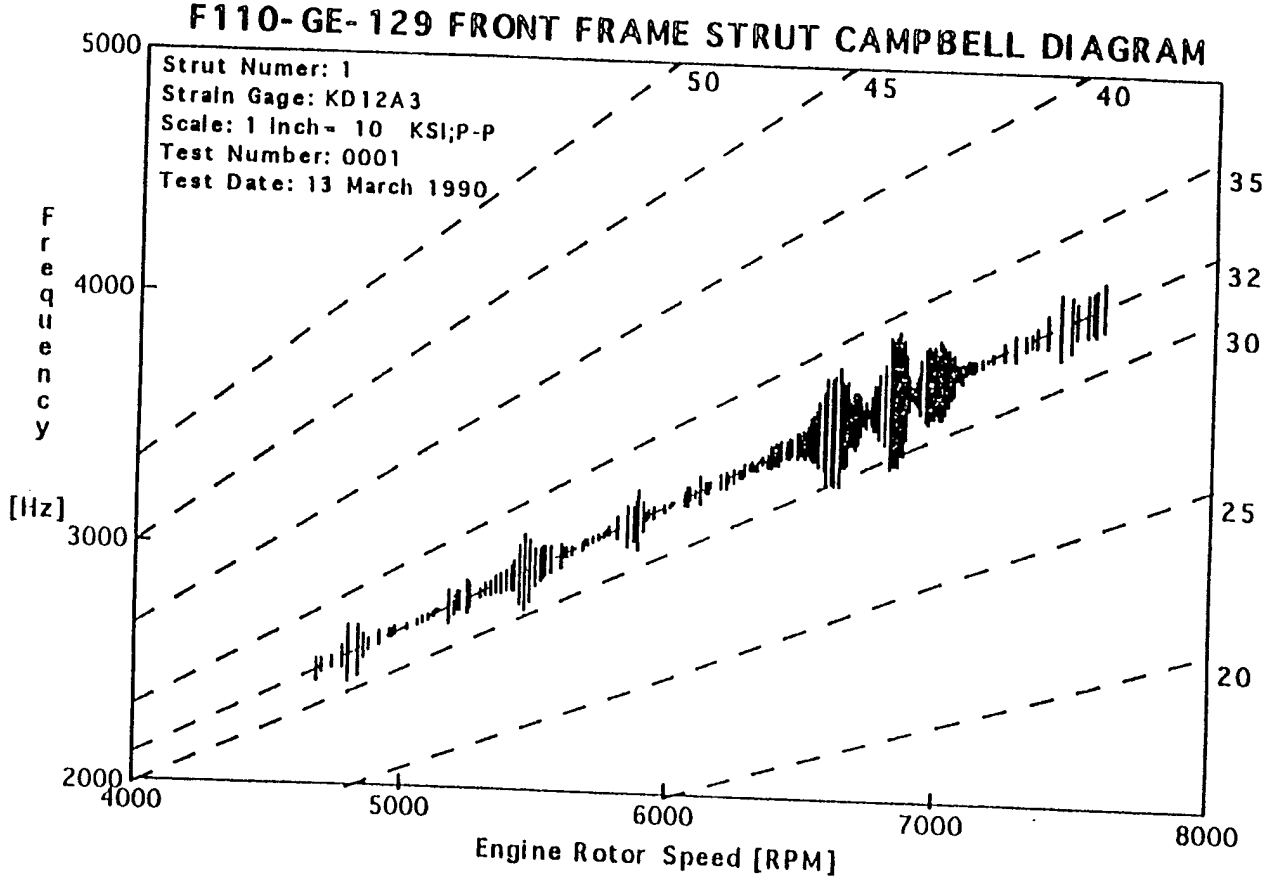

Figure 3. Campbell diagram for KD12A3. Engine working condition: P_1=24 psia, T_1=60 °F. IRIG time: 072:10:15:47 -- 072:10:18:49.

WP PROJECT, STUDENT RESEARCH SCHEDULE

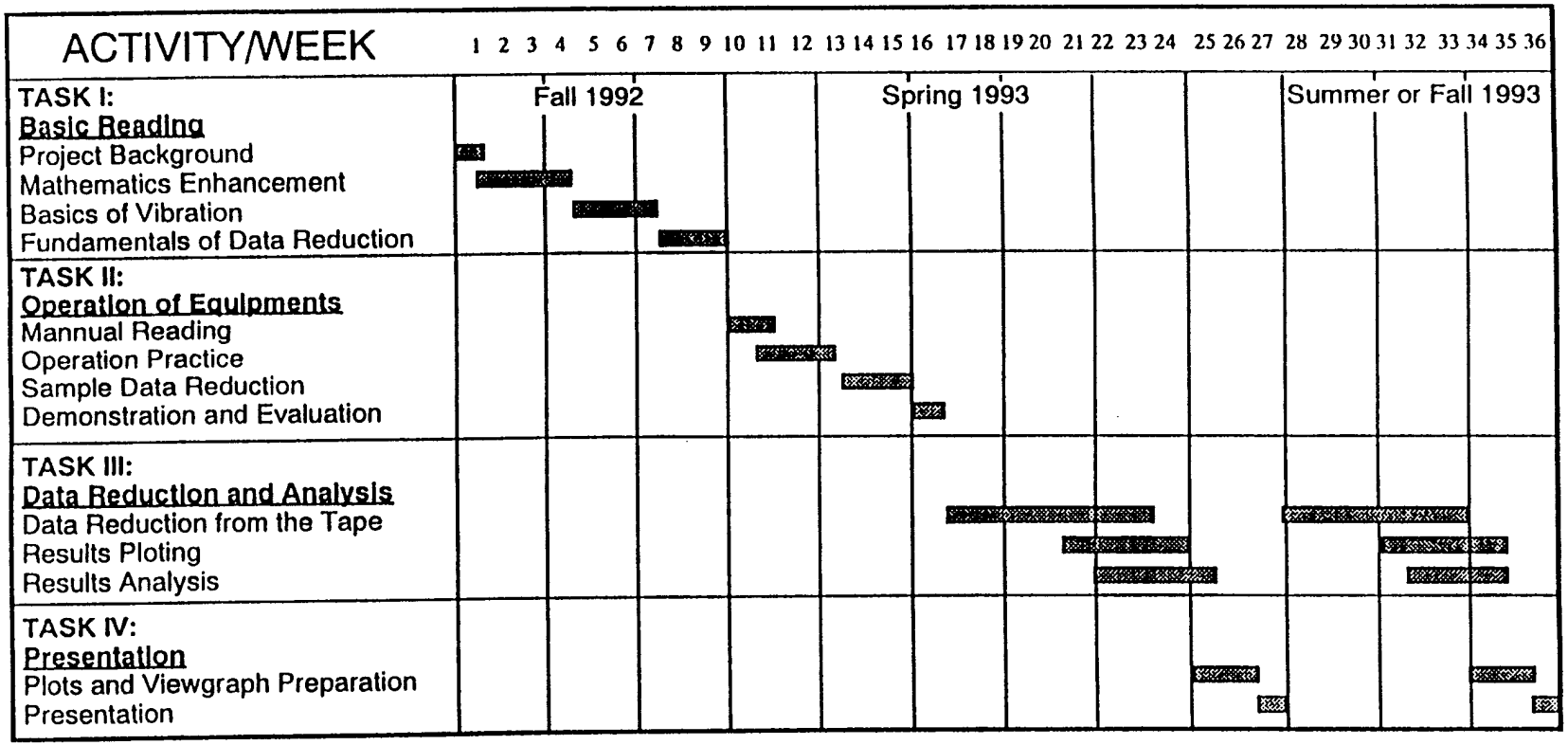

Bi-weekly Report on Due: • • • • • • • • • • • • • • • • • •

Wright Patterson Project

BIWEEKLY RESEARCH PROGRESS REPORT

For Period:_____ to _____ Name:_____

1. In the space below briefly describe your project related activities for the indicated period. Please describe work in progress, any results and number of hours spent during the period. Write on back of this page if additional space is needed.

2. Do you have any difficulties? If yes, please describe. Do you need any extra help? On what matter?

3. Briefly describe your work plan for the next two weeks.

UNDERGRADUATE RESEARCH EXPERIENCE

PROJECT REPORT SUMMARY

Researcher: Dolon D. Silimon
Mentor: Dr. Bai

May 4/93

We are involved with research in Structural Dynamics and Control and Aeropropulsion, which deals with aeroengine, specifically with the investigation of the causes of the catastrophic fatigue failure of struts in the front frame of certain Air Force jet engines.

There are several basic research issues which we examined in this part of the project. The effective damping of the front frame struts include the inherent structural damping, as well as the energy exchange between the vibrating struts and the duct acoustics modes.

The project we are working on covers four tasks. Task I is Basic Reading, which covers project background, mathematics enhancement, basics of vibration, and fundamentals of data reduction. Task II is Operation of Equipments, which covers manual reading, operation practice, sample data reduction, and demonstration and evaluation. Task III is Data Reduction and Analysis, which covers data reduction from the tape, results plotting, and results analysis. Task IV is Presentation, which covers plots, viewgraph preparation, and the presentation itself.

The object of the project is to reduce and analyze aeromechanical test data obtained from full scale engine tests at AEDC; to investigate the causes for excessive vibration response of the front frame struts of the F110-GE-129 high performance turbofan engine; and to develop analytical and/or empirical models for predicting the conditions under which such high responses occur, with the aim of discovering ways of

Designing jet engine to be free of such vibration problems.

In the first months of our research experience we were conducted through seminars(twice a week) and through the three projects for our participation. These projects include: (1) Reduction of Example Test Data from Analog Tapes; (2) Analyses of F110-GE-129 Front Frame Campbell Diagrams; and (3) Analyses of F110-GE-129 Front Frame Siren Test Data. From these projects we produced some preliminary results.

In the first three months of our research experience we completed our Project Background and Mathematics Enhancement sections, under the supervision of Dr. Singh(mentor). We covered the section of Free Oscillations, in which we wanted to determine the motion of our mechanical system, that is, the displacement of the body as a function of time. We studied Fourier Series and Integrals, which included: Periodic Functions, Trigonometric Series, Euler's formulas, even and odd functions, functions having arbitrary period, half-range expansions, determining fourier coefficients without integration, and Forced Oscillations.

In the month of February we switched mentors from Dr. Singh to Dr. Talukder. With Dr. Talukder we worked diligently to apply differential equations to understand vibrations. We worked on, free vibration, damped vibration(three cases of damped vibration), and forced vibrations. Forced vibration is a combination of phenomenon described by the particular and

transient solutions(which vanishes after a short period of time). To end the work with Dr. Talukder we talked about the difference between damping and no damping in a system, and how to tell if a situation is a super-critical, critical, and undercritical situation. We talked about resonance which is the dramatic increase in amplitude near to its own natural frequency. When the system is resonating, it responds by oscillating with a relatively large amplitude.

Through our concluding months we worked with Dr. Bai as our mentor, which was the beginning of Task II which is the Operation of Equipment. In these final months we processed the strain gauge signals by the use of the commercial program provided by Hewlett Packard 3566A. The signal was already downloaded from the magnetic tape and digitized. It was required that the time domain signals be FFT analyzed to obtain their linear spectrum. Starting from the time 7.5 sec. until time 15 sec., we had to specify a .25 sec. fraction of the signals once a time, perform FFT/Linear Spectrum for channel 1 to channel 7. We recorded the peak value(in mV), its frequency(in Hz) and the next highest peak(in mV), and its frequency(in Hz). Perform FFT/Linear Spectrum for channel 8. Record only the location(in Hz) of the peak value. Then we moved to the next. 25 sec. and continued the process until we finished the whole section.

The next phase Dr. Bai had us work on is called Phase

III, Data Reduction. To complete this stage we had to use the Macintosh computer. We were encouraged to go to the library for reference books on Excel and Quick BASIC. In this phase we had to complete four tasks. The first task included learning how to use a spreadsheet program, Microsoft Excel, on the Macintosh computer. Task two was to prepare, using Excel, the file for the Campbell diagram plotting program. Task three was to learn Quick Basic programming language. In task four we are to study the plotting program in our packet, which was written in Quick BASIC for Macintosh.

Appendix B

Copy of AIAA Paper 93-1873.

AIAA 93-1873
Aero-Engine Component Damping Estimation From Full-Scale Aeromechanical Test Data

J. A. Fabunmi
AEDAR Corporation
Landover, MD

T. Bai, O. Puri, K. Bota
Clark Atlanta University
Atlanta, GA

Lt. Carolyn Sunderland
WL/POTX
Wright-Paterson AFB, OH

AIAA/SAE/ASME/ASEE
29th Joint Propulsion Conference and Exhibit
June 28-30, 1993 / Monterey, CA

AERO-ENGINE COMPONENT DAMPING ESTIMATION FROM FULL-SCALE AEROMECHANICAL TEST DATA

James A. Fabunmi*, Tiejun Bai**, Om Puri+, Kofi Bota#
and
Lt. Carolyn Sunderland, USAF++

Abstract

The forced response measurements from strain gages during engine aeromechanical testing contain information which can reveal the effective damping of the component's resonant modes. Knowledge of the effective damping is important for detecting trends in the fluid/structure interaction during operation. This paper presents the formulation and application of techniques which have previously been developed for modal testing and analysis, to the analysis of the forced response of structural components of high performance aircraft jet engines. Time traces of strain gage data are transformed into linear spectra by Fast Fourier Transform (FFT). Zoom FFT transforms in the neighborhood of a resonant frequency are used to fit modal circles. This local spectrum technique is valid under the assumptions that the modes are separated well enough and are lightly damped. It is also assumed that the spectra of the excitation forces does not vary rapidly near the resonant frequency. Using data gathered from full scale engine aeromechanical tests, it is shown that these assumptions are plausible, and that the proposed technique is feasible for estimating the modal damping of engine components from forced vibration data.

Nomenclature

A, B, C, E, F	Quantities defined in Eq. 21 through 25
$A_{ij_n}(\omega)$	Quantity defined in Eq. 4
a, b	Coordinates of center of modal circle
$B_{ij_n}(\omega)$	Frequency function defined in Eq. 6
e, f	Quantities defined in Eq. 19 and 20
$f(\omega)$	Spectra of excitation forces
$f_j(\omega)$	j-th Excitation force
$G_n(\omega)$	Frequency function defined in Eq. 7
$g, g(\omega)$	Damping coefficient
Im( )	Imaginary part
M	Dimension of excitation force vector
m_n	n-th Modal mass
N	Dimension of forced response vector
Re( )	Real part
$Y(\omega)$	Matrix of frequency response functions
$Y_{i,j}(\omega)$	i,j-th Frequency response function
$y(\omega)$	Spectra of forced responses
$y_i(\omega)$	i-th Forced response
$\{\phi\}$	Orthonormal mode vector
θ_{+}, θ_{-}	Angles defined in Eq. 17 and 18
Ω, Ω_n	Natural frequency

Introduction

Forced response problems in high performance aircraft engines have remained major obstacles to the development of high performance, light-weight engines. Over the past several decades, considerable research effort has been devoted to the forced response and fluid-structural instabilities of rotating components such as fan, compressor and turbine rotor systems as well as the non-rotating components such as stators.

Excessive stress levels can occur in engine components due to interactions between the structure and the unsteady flow field in the duct. Although measures have been taken which increase the structural damping of these components, the physical mechanisms responsible for this problem are yet to be fully understood. By inverse reasoning, if the fix to the problem is to apply damping treatments to the components, then whatever is happening during engine operation must be having the effect of reducing the effective damping of the structure. It is of interest to investigate how the effective damping of the engine structural components varies with engine operating conditions. Our approach to this investigation is to examine ways of identifying the effective damping at different operating conditions.

This work is motivated by efforts to understand the causes of excessive vibrational stresses which have resulted in premature failures of the front frame struts of certain high performance aircraft jet engines. In order to isolate the trends in the occurrence of these unusually high stresses, it is necessary to obtain estimates of the effective damping of the structure at different engine operating conditions. The conventional processing of engine aeromechanical data e.g. Campbell Diagrams etc., do not provide this information. However, it is evident that the forced response data measured while the engine is undergoing aeromechanical testing, may contain sufficient information to estimate the effective damping of the resonant modes. A study of the trends in these damping factors should reveal the possible conditions under which the struts can be expected to experience increased vibrational stresses. In this paper, certain assumptions which appear valid for the operation of jet engines, permit the application of techniques which have previously been used to identify modal damping from measurements of structural transfer functions. The key idea is to recognize that although the measured responses themselves are not transfer functions, if the spectra of the excitation forces are nearly uniform, the nature of the forced response spectra in the complex plane, is very similar to that of transfer functions. This requirement is met by the fact that the forced responses of the engine stationary components are derived from engine order excitations whose spectra vary with the engine rpm. Therefore, as the rpm is steadily increased from low to high (or from high to low), the effective excitation of the engine components are similar to that of a swept sine excitation in modal testing. In the complex plots of the linear forced response spectra, the role of modal constant is played by an unknown quantity (consisting of the modal constant and the unknown excitation) which needs not be determined in order to extract the modal damping factor.

* President, AEDAR Corporation, Landover Maryland, Member AIAA
** Research Scientist, Clark Atlanta University, Atlanta, Georgia, Member AIAA
+ Professor of Physics, Clark Atlanta University, Atlanta, Georgia
# Vice President for Research, Clark Atlanta University, Atlanta, Georgia
++ Aeropropulsion Laboratory, Wright Laboratories, Dayton Ohio

Modal Damping Estimation Theory

The analysis of frequency response data to obtain modal properties was first developed by [Kennedy and Pancu, 1947] in their work on aircraft flutter testing. Advances made in this field in recent years have been due to the ready availability of powerful computational resources for the rapid analysis of fast Fourier transforms. The detailed theory of modal testing and analysis have been presented in several publications e.g. [Lang, 1975], [Brown et al, 1977], [Ewins, 1984], [Flannelly, Nagy and Fabunmi, 1981], [Fabunmi and Tasker, 1988]. By starting with the forced responses in the frequency domain, expressed in terms of the mobility functions and the excitation forces, equations which have previously been used to analyze frequency response functions, are applied to the linear spectra of the forced responses themselves, in order to estimate the modal damping factors.

The linear spectra of the forced responses of a damped structure can be related to the spectra of the excitation forces via the frequency response functions:

$$\{y(\omega)\} = [Y(\omega)]\{f(\omega)\} \tag{1}$$

where $\{y(\omega)\}$ is the N x 1 vector of the forced response, $\{f(\omega)\}$ is the M x 1 vector of the excitation forces, and $[Y(\omega)]$ is the N x M matrix of the structural frequency response functions. In other words, the response spectra at coordinate i due to forces at all the M excitation coordinates is given by:

$$y_i(\omega) = \sum_{j=1}^{M} Y_{ij}(\omega) f_j(\omega) \tag{2}$$

For a fairly general class of damping mechanisms, the expression for the matrix $[Y(\omega)]$ has been shown to be [Fabunmi, 1985]:

$$\{Y(\omega)\} = \sum_{n=1}^{N\to\infty} \left[\frac{\{\phi\}_n\{\phi\}_n^T}{m_n}\right] \frac{1}{\Omega_n^2(1-(\omega^2/\Omega_n^2)+ig_n(\omega))} \tag{3}$$

where $\{\phi\}_n$ is the n-th orthonormal mode vector of the structure, $\{\phi\}_n^T$ is its transpose, m_n is the n-th modal mass, Ω_n is the frequency of the n-th mode, and $g_n(\omega)$ is the frequency dependent damping coefficient of the n-th mode. If the element (i, j) of the matrix $\left[\frac{\{\phi\}_n\{\phi\}_n^T}{m_n}\right]$ is demoted by A_{ijn}, then:

$$Y_{ij}(\omega) = \sum_{n=1}^{N\to\infty} \frac{A_{ijn}}{\Omega_n^2(1-(\omega^2/\Omega_n^2)+ig_n(\omega))} \tag{4}$$

and the forced response at coordinate i become:

$$y_i(\omega) = \sum_{j=1}^{M} \sum_{n=1}^{N\to\infty} \frac{A_{ijn} f_j(\omega)}{\Omega_n^2(1-(\omega^2/\Omega_n^2)+ig_n(\omega))} \tag{5}$$

Further, let:

$$B_{in}(\omega) = \sum_{j=1}^{M} \frac{A_{ijn} f_j(\omega)}{\Omega_n^2} \tag{6}$$

and,

$$G_n(\omega) = \frac{1}{1-(\omega^2/\Omega_n^2)+ig_n(\omega)} \tag{7}$$

then the forced response at coordinate i can be written as:

$$y_i(\omega) = \sum_{n=1}^{N\to\infty} B_{in}(\omega) G_n(\omega) \tag{8}$$

At frequencies close to the resonance of mode n, the forced response is dominated by the contribution of that made to the series in Eq. 8. In the neighborhood of this frequency, following the assumption that the spectra of the excitation forces does not vary sharply with frequency, the forced response can therefore be approximated by the following expression:

$$y_i(\omega) = B_{in}(\omega) G_n(\omega) + \varepsilon_n \qquad (\Omega_n - \Delta < \omega < \Omega_n + \Delta;\ \ \Delta \to 0) \tag{9}$$

where ε_n is a complex valued residual due to the contributions of the remaining truncated modes. All the quantities in Eq. 9 are complex valued, and in the neighborhood of the resonant frequency Ω_n, the frequency behavior of $G_n(\omega)$governs the frequency behavior of the forced response. It will further be assumed that the damping function $g_n(\omega)$ appearing in the definition of $G_n(\omega)$ is approximated by its value at $\omega = \Omega_n$, thus:

$$G_n(\omega) = \frac{1}{1-(\omega^2/\Omega_n^2)+ig_n(\Omega)} \tag{10}$$

In the subsequent discussions, $g_n(\Omega)$ will be referenced simply as g_n, the damping coefficient of the n-th mode. The function represented by Eq. 10 has been the subject of extensive analysis in publications on the subject modal testing and analysis. The following is a brief review of its more relevant properties. The real and imaginary parts of $G_n(\omega)$ are:

$$\mathrm{Re}(G_n(\omega)) = \frac{1-(\omega^2/\Omega_n^2)}{(1-(\omega^2/\Omega_n^2))^2+g_n^2} \tag{11}$$

$$\mathrm{Im}(G_n(\omega)) = \frac{-g_n}{(1-(\omega^2/\Omega_n^2))^2+g_n^2} \tag{12}$$

It follows that:

$$\mathrm{Re}(G_n(\omega))^2 + \mathrm{Im}(G_n(\omega))^2 = -\frac{\mathrm{Im}(G_n(\omega))}{g_n} \tag{13}$$

or,

$$\mathrm{Re}(G_n(\omega))^2 + \left(\mathrm{Im}(G_n(\omega)) + \frac{1}{2g_n}\right)^2 = -\frac{1}{4g_n^2} \tag{14}$$

On a Nyquist plot of $G_n(\omega)$, with $\mathrm{Im}(G_n(\omega)$ as ordinate and $\mathrm{Re}(G_n(\omega))$ as abscissa and frequency as parameter, according to Eq. 14, a circle will be obtained. Its center will be at coordinate $(0, -\frac{1}{2g_n})$, and its radius will be $\frac{1}{2g_n}$. For any pair of points on the circle, lying on opposite sides of the resonant frequency, the damping coefficient can be expressed as follows:

$$g_n = \frac{\omega_+^2 - \omega_-^2}{\Omega_n^2(\tan(\theta_+) + \tan(\theta_-))} \tag{15}$$

From Eq. (9), the arc of the Nyquist plot of the forced response spectra will be part of a circle which has been amplified by a factor of $|B_{in}(\omega)|$, rotated about the origin through an angle of $\arg(B_{in}(\omega))$ and then shifted from the origin by the complex residual ε_n (see Fig. 2). The circle that is fitted to the data in the neighborhood of the resonant frequency will have an origin at some coordinate (a,b). The point on this circle, diametrically opposite the resonant frequency will have coordinate (e,f). If the forced response data in the neighborhood of the resonant frequency are represented by an ordered set of numbers denoted by:

$$(\omega_i; \mathrm{Re}(y(\omega_i)); \mathrm{Im}(y(\omega_i)));$$
$$i = -L, -(L-1), \ldots\ldots -1, 0, 1, \ldots\ldots L-1, L; \quad \omega_0 = \Omega_n;$$

then following are the necessary formulas needed to identify the modal damping from the forced response spectra (see Fig. 2):

$$g_n^{i,j} = \frac{\omega_{+i}^2 - \omega_{-i}^2}{\Omega_n^2(\tan(\theta_{+i}) + \tan(\theta_{-i}))} \tag{16}$$

where:

$$\theta_{+i} = \arccos \frac{[\mathrm{Re}(y(\omega_{+i})) - e][\mathrm{Re}(y(\Omega_n)) - e] + [\mathrm{Im}(y(\omega_{+i})) - f][\mathrm{Im}(y(\Omega_n)) - f]}{\sqrt{\{[\mathrm{Re}(y(\omega_{+i})) - e]^2 + [\mathrm{Im}(y(\omega_{+i})) - f]^2\}\{[\mathrm{Re}(y(\Omega_n)) - e]^2 + [\mathrm{Im}(y(\Omega_n)) - f]^2\}}} \tag{17}$$

$$\theta_{-i} = \arccos \frac{[\mathrm{Re}(y(\omega_{-i})) - e][\mathrm{Re}(y(\Omega_n)) - e] + [\mathrm{Im}(y(\omega_{-i})) - f][\mathrm{Im}(y(\Omega_n)) - f]}{\sqrt{\{[\mathrm{Re}(y(\omega_{-i})) - e]^2 + [\mathrm{Im}(y(\omega_{-i})) - f]^2\}\{[\mathrm{Re}(y(\Omega_n)) - e]^2 + [\mathrm{Im}(y(\Omega_n)) - f]^2\}}} \tag{18}$$

$$e = 2\left(\frac{BE - CF}{AB - C^2}\right) - \mathrm{Re}(y(\Omega_n)) \tag{19}$$

$$f = 2\left(\frac{AF - CE}{AB - C^2}\right) - \mathrm{Im}(y(\Omega_n)) \tag{20}$$

$$A = \sum_{i=-L}^{L} 4[\mathrm{Re}(y(\omega_i)) - \mathrm{Re}(y(\Omega_n))]^2 \tag{21}$$

$$B = \sum_{i=-L}^{L} 4[\mathrm{Im}(y(\omega_i)) - \mathrm{Im}(y(\Omega_n))]^2 \tag{22}$$

$$C = \sum_{i=-L}^{L} 4[\mathrm{Re}(y(\omega_i)) - \mathrm{Re}(y(\Omega_n))] \times [\mathrm{Im}(y(\omega_i)) - \mathrm{Im}(y(\Omega_n))] \tag{23}$$

$$E = \sum_{i=-L}^{L} 2[\mathrm{Re}(y(\omega_i)) - \mathrm{Re}(y(\Omega_n))][\{\mathrm{Re}(y(\omega_i))^2 - \mathrm{Re}(y(\Omega_n))^2\} + \{\mathrm{Im}(y(\omega_i))^2 - \mathrm{Im}(y(\Omega_n))^2\}] \tag{24}$$

$$F = \sum_{i=-L}^{L} 2[\mathrm{Im}(y(\omega_i)) - \mathrm{Im}(y(\Omega_n))][\{\mathrm{Re}(y(\omega_i))^2 - \mathrm{Re}(y(\Omega_n))^2\} + \{\mathrm{Im}(y(\omega_i))^2 - \mathrm{Im}(y(\Omega_n))^2\}] \tag{25}$$

The superscript "i,j" in Eq. 16 has been used to underscore the fact that due to the imperfection of measured data, and the approximate nature of the circle fit technique, the value of the damping coefficient calculated using different pairs of points on either side of the resonant frequency, will differ slightly from each other. If all possible combinations of i,j are used, then a statistical technique can be used to determine the mean value of the damping coefficient, as well as its standard deviation.

Data Reduction System

The data processing system used for this research accepts pre-recorded data from full-scale engine aeromechanical tests in the form of analog magnetic tapes. The system consists of the data reproduction and the data analysis systems (see Figure 3). The engine test data are the strain-gage measurements recorded on 14-track, 1-in. analog magnetic tapes. To reproduce these data, a METRUM (HONEYWELL) Data Storage Model 101e Portable Tape System is used. The tape system is a high-performance, IRIG, portable, magnetic tape record/reproduce system with microcomputer control. The system uses 1 inch wide magnetic tape with maximum reel size of 15 inches. It has a 14 track head configuration, among them 12 channels that can be set as FM channels and 2 as direct-record channels. It has a self-contained calibration system and can automatically conduct calibration verification. Though the system is portable, it provides nearly equal performance as full-size laboratory recorders. For FM record/reproduce, its linearity is 0.5% of full deviation from best straight line through zero. The harmonic distortion is 1.2% maximum. In addition, the operation of the system can also be controlled by an external computer through the RS-232 computer interface.

The data analysis system is a 386sx based computer system interfaced with a Multichannel Spectrum/Network Analyzer--HP 3566A. The tape recorded data are reproduced by the tape system and then acquired by the computer controlled analyzer for further analysis. The core of the data analysis system is the Multichannel, Spectrum/Network Analyzer--HP 3566A (see Figure 3). This analyzer is a powerful time and frequency domain measurement tool, which offers features for all types of mechanical testing, including rotating machinery analysis, vibration test, structural analysis and acoustic noise testing. The analyzer is linked to a 386sx computer, HP Vectra QS/16S, which controls the operation of the analyzer and performs the data analysis and other operations. The analyzer has 8 channels that acquire data simultaneously. For fast measurement processing, a powerful hardware signal processor module converts time data to frequency data using FFT technology. The analyzer has a dynamic range of 72 dB and maximum frequency span of 12.8 kHz. It can acquire data at a maximum rate of 32,768 samples/sec per channel with a cross channel accuracy of 0.1dB (plus or minus).

The first step in estimating the damping coefficients identification is to run zoom FFT on the raw signals. The capability to zoom allows closely spaced measurement points over a narrower band. The measurement resolution is increased and the distortion due to leakage is also reduced because the smearing of energy is now within a narrower bandwidth. In order to run zoom FFT for a time captured file, which stores the raw signals from the strain gauges, the frequency band must be specified when the signals are acquired from the tape to generate the time captured data file. Since this frequency band is not known beforehand, the signals are first acquired using wide band settings, which are usually from 0Hz to 12.8kHz. A typical raw signal trace acquired by the wide band settings is shown in Figure 4. This data file is then FFT analyzed to determine the frequencies at which high amplitude resonance occurred. Next, these frequencies are used as center frequency

and a narrow frequency span is specified to acquire the raw signals once again. The time trace from a typical time captured data file generated by using the narrow band settings is shown in Figure 5 and this is the data file that will be used for the zoom FFT analysis.

Results

Figures 6 through 8 present the results obtained from the zoom FFT analysis with a frequency span of 100 Hz. These results include the magnitude of the linear spectrum (Fig. 6), the real part of the linear spectrum (Fig. 7) and the imaginary part (Fig. 8). Examination of Figure 6 shows that the magnitude of the dynamic stress has a maximum close to 3140 Hz, which is a indication of a resonant mode of the structure. However, there exists another magnitude peak at about 3143 Hz, which suggests the existence of another mode. Therefore, to obtain the damping coefficient for the 3140 Hz mode, only the data around this center frequency will be used in the circle fitting process.

In Figure 9, the Nyquist plot which covers the frequency range from 3138 Hz to 3142 Hz is presented along with a sketch which shows the circle fitting results. The Nyquist plot was produced by plotting the data points and curve fitting them with a spline. Examination of this figure indicates that the Nyquist plot based upon the data in this frequency range indeed qualitatively resembles the shape of a circle. The zoom FFT results in this frequency range are then used to determine the center point coordinate, (a, b), the radius of the circle and the damping coefficient which is expressed as g(Ω). The results from this process are shown on the right side of the figure.

Conclusions

The research effort reported in this paper has established the feasibility of estimating modal damping of aeroengine structural damping components from strain-gage time histories measured during full-scale aeromechanical testing. A data reduction and analysis system capable of reproducing and analyzing pre-recorded test data from analog tapes, has been used to demonstrate a concept based on fitting modal circles to zoom FFT of forced responses of engine structural components. Under the assumptions that the spectra of the excitation sources are nearly uniform compared to the spectra of the responses near the resonances of the structural modes, the circle fitting technique which is well established for analyzing frequency transfer functions, proves to be just as effective for estimating modal damping from forced response data. Data from actual engine aeromechanical tests were used validate the applicability of this approach. Future efforts will include the detailed study of damping trends of aeroengine structural components under various engine operating conditions.

Acknowledgments

This research was sponsored by the Aeropropulsion Directorate of the United States Air Force Wright Laboratories. The United States Government is authorized to reproduce and distribute reprints for governmental purposes notwithstanding any copyright notation herein.

References

Brown, D., Carbon, G. and Ramsey, K. 1977. "Survey of Excitation Techniques Applicable to the Testing of Automotive Structures," Proceedings SAE, No. 770029.

Ewins, D.J. 1984. "Modal Testing: Theory and Practice," Research Studies Press.

Fabunmi, J.A. 1985. "Extended Damping Models for Vibration Data Analysis," Journal of Sound and Vibration (1985) 101(2), pp. 181-192.

Fabunmi, J.A. and Tasker, F.A. 1988. "Advanced Techniques for Measuring Structural Mobilities," Proc. ASME Journal of Vibration, Acoustics, Stress, and Reliabilities in Design, Vol. 110, pp. 345-349.

Flannelly, W.G., Nagy, E.J. and Fabunmi, J.A. 1981. "Analytical Testing," NASA CR 4329, May 1981.

Kennedy, C.C. and Pancu, C.D.P. 1947. "Use of Vectors in Vibration Measurement and Analysis," Journal of the Aeronautical Sciences, Vol. 14, No. 11, Nov. 1947.

Lang, G.F. 1975. "Understanding Vibration Measurements," Application Note No. 9, Nicolet Scientific Corporation.

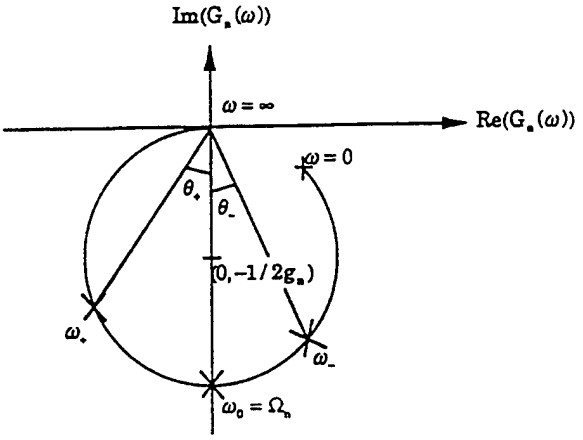

Figure 1. Nyquist plot of the frequency function $G_n(\omega)$.

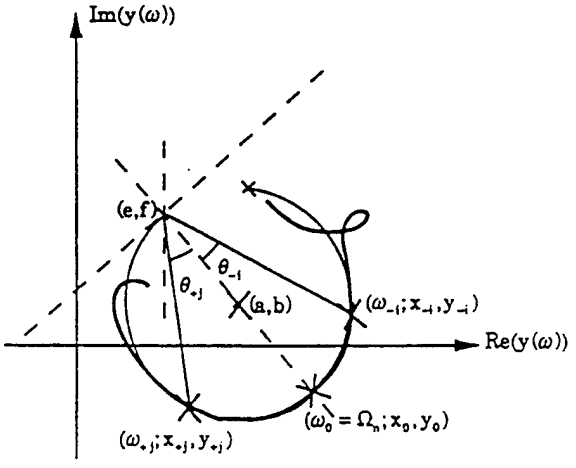

Figure 2. Nyquist plot of the forced response spectra.

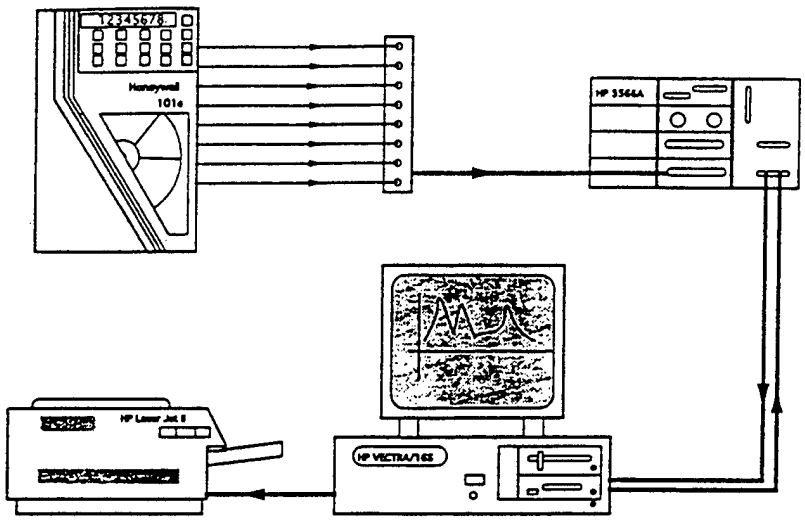

Figure 3. Schematic of the Multi-Channel, Spectrum/Network Analyzer and the tape record/reproduce system.

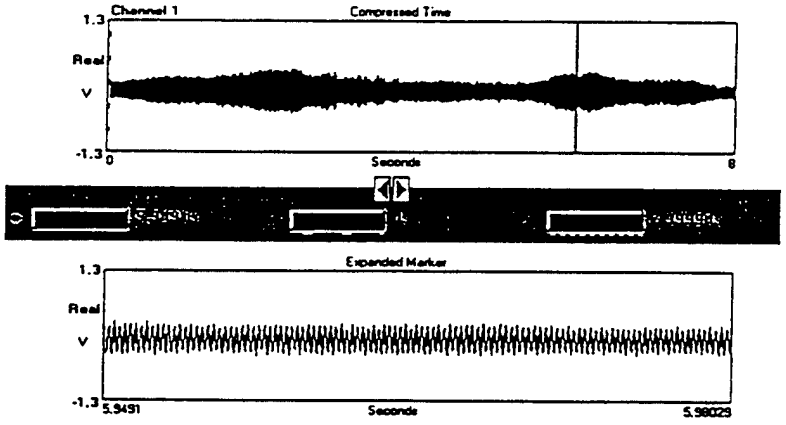

Figure 4. Time trace of raw strain gage signals. The signals were acquired using a frequency setting of 0 to 12.8 kHz.

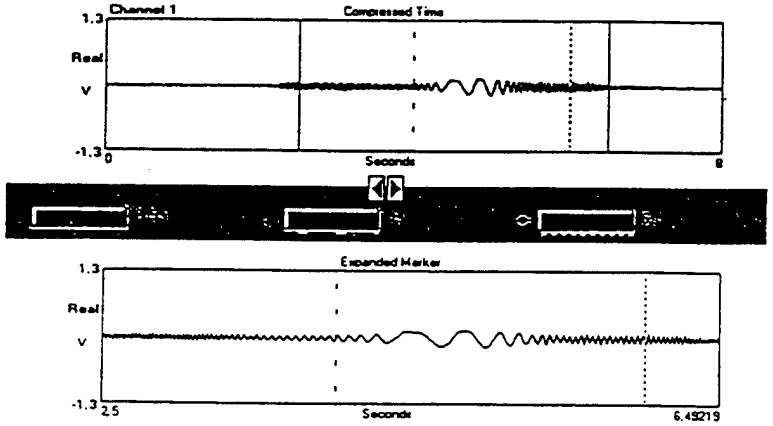

Figure 5. Time trace of raw strain gage signals. The signals were acquired using a center frequency 3633 Hz with a span of 100 Hz.

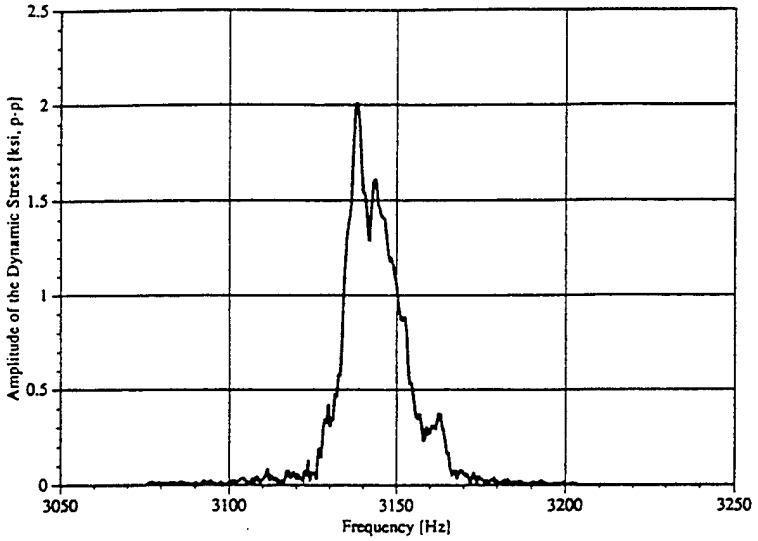

Figure 6. The magnitude of the linear spectrum of a strain gage signal with center frequency of 3150 Hz.

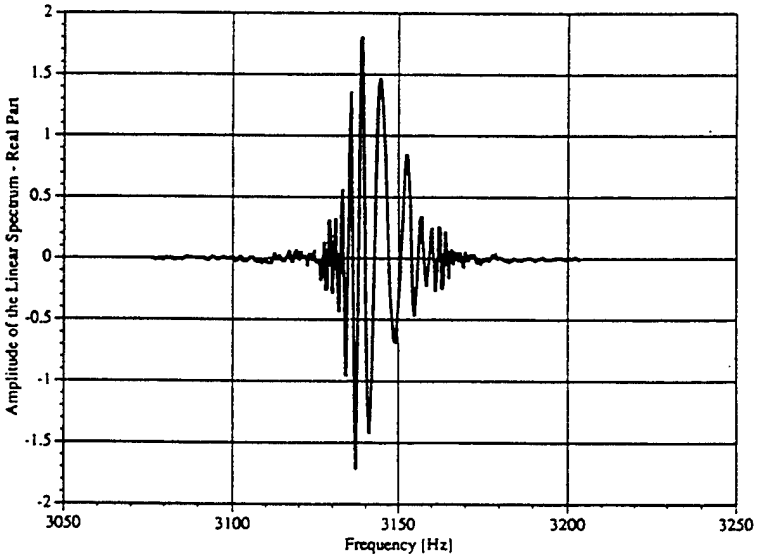

Figure 7. The real part of the linear spectrum of Figure 6.

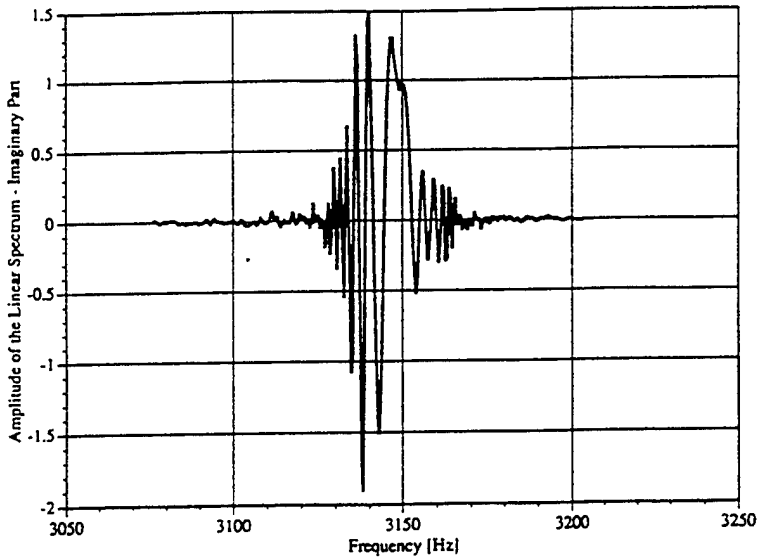

Figure 8. The imaginary part of the linear spectrum of Figure 6.

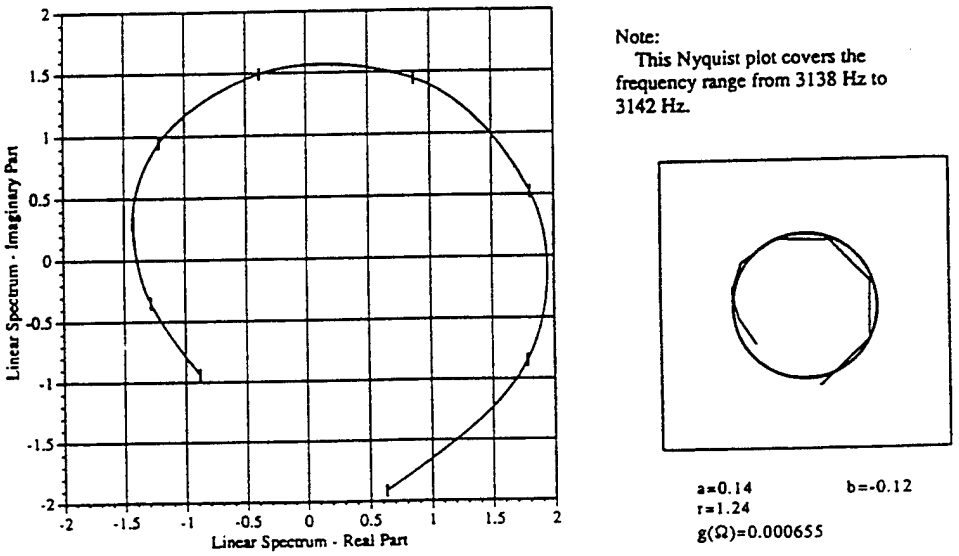

Figure 9. The Nyquist plot of the linear spectrum of Figure 6.

Appendix C

Copy of AIAA Paper 95-0724.

AIAA 95-0724
An Analysis of Aeroelastic Response of Vibrating Surfaces

Frederick Ferguson and James Fabunmi
AEDAR Corporation, Landover, MD

Tiejun Bai
Clark Atlanta University, Atlanta, GA

33nd AIAA Aerospace Sciences Meeting and Exhibit

January 9-12, 1995 / Reno, NV

An Analysis of the Aeroelastic Response of Vibrating Surfaces

By
Frederick Ferguson, Ph. D., and James Fabunmi, Ph. D., PE
AEDAR Corporation, 8401 Corporate Drive, Suite 460, Landover, MD 20785

and

Tiejun Bai, Ph.D.
Clark Atlanta University, Atlanta, GA.

Abstract

A theoretical study of the phenomena which exhibit appreciable reciprocal static and dynamic interaction between the aerodynamic forces and the elastic behavior of vibrating surfaces is conducted. The perturbation on the transverse motion of a uniformly parallel gas stream due to the vibration of an idealized plate is analyzed. Analytical solutions are obtained for the perturbed flow field parameters for a class of prescribed vibratory motion of the plate. Particular attention is given to the aerodynamic characteristics of the flow that is responsible for transferring mechanical energy from the transverse flow field to the vibrating surface. The conditions under which mechanical energy is extracted from the flow field inorder to maintain and possible amplify the vibratory motion of the elastic surface is determined.

1. Introduction

The design of complex vehicles, such as the supersonic aircraft and the high subsonic civil transport (HSCT), to satisfy certain flutter constraints is greatly hampered by the inherent difficulties and cost of detailed flutter analyses. Panel flutter, which is the self-excited oscillation of a plate or shell when exposed to an airflow along its surface, is an inherent feature of all flight vehicles. Practical flight tests and experimental observations have confirmed that this form of excitation can lead to structural failures. Therefore, detailed knowledge of the critical dynamic pressures and other conditions under which the plate motion becomes unstable are vital to aircraft designers.

The analysis conducted in this paper is based on the worked presented in References 1 and 2. An analytical evaluation of the aeroelastic nature of panel flutter is conducted. Particular attention is given to the aerodynamic characteristics of the flow, and the panel modes of vibrations that leads to flutter The present analysis will be restricted to the small disturbance equations coupled with boundary conditions in the form of plane waves.

2. Statement of Aeroelastic Problem

Consider a uniform flow over a vibrating surface as depicted in figure 1. Assume that the surface is vibrating in the direction of the y-axis while the gas flow is moving along the x-axis. The

coordinate system xyz is fixed. The uniform flow is parallel to the xz-plane.

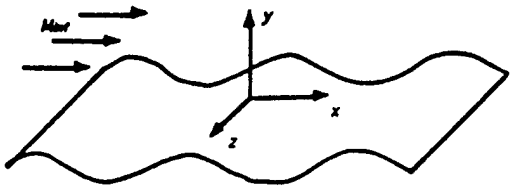

Figure 1. Illustration of uniform flow over vibrating surface

The displacement of the vibrating surface in the direction of the y-axis is represented by ξ. The elements of the elastic surface vibrate with the frequency ω in the direction of the y-axis. The period of vibration, T, is given as

$$T = \frac{2\pi}{\omega}$$

The wavelengths of a single wave pocket in the x and z-directions are defined as λ_x and λ_z. The symbol Δp represents the pressure disturbances due to the vibratory motion of the elastic surface.

The goal of this analysis is to determine the influence of the flow on the motion of the vibrating surface as it transverse the length of the plate. In particular the following questions will be answered: Under what conditions does the flow transfer energy into the vibratory motion of the plate? Does the flow experiences wave drag or thrust? Does the amplitude of vibration of the plate grows or diminishes?

3. Analytical Evaluation

In developing a theoretical model for analyzing the interaction of the gas flow and the elastic surface, the following definitions are warranted:

Definition 1: Mechanical Force

The mechanical force, f, acting on an element of the elastic surface, ds, due to the motion of the gas flow is defined as

$$f = \Delta p ds = \Delta p dx dz$$

where Δp is the net pressure acting on the surface element.

Definition 2: Displacement of Surface Element

The interaction of the gas flow and the elastic surface result in a displacement, dl, of the surface element, which is represented by

$$dl = \frac{\partial \xi}{\partial t} dt$$

Definition 3: Resistance Force on Surface Element

Each surface element produces a resistance force, r, for every corresponding displacement. The resistance force on an element of the elastic surface is defined by

$$r = \Delta p \frac{\partial \xi}{\partial x} dx dz$$

Definition 4: Average Density of Mechanical Energy Flux

The average density of mechanical energy flux, dE (measured in $W m^{-2}$) acting on a single wave packet over the period of vibration, T, is determined by the integral

$$\begin{aligned} dE &= \frac{1}{\lambda_x \lambda_z T} \iint_{\text{wave packet}} \bar{f} \cdot d\bar{l} \\ &= \frac{\omega}{2\pi \lambda_x \lambda_z} \int_0^T \int_0^{\lambda_x} \int_0^{\lambda_z} \Delta p \frac{\partial \xi}{\partial t} dx dz dt \end{aligned} \qquad (1)$$

Energy flux must be expended from the flow, ie., $E > 0$, to make one square meter of the elastic surface vibrate with the frequency ω.

Definition 5: Specific Wave Resistance

The specific wave resistance, dR_x, (measured in $N m^{-2}$ or Pa) along the x-axis averaged over the period, T, is

represented by the integral

$$dR_x = \frac{1}{\lambda_x \lambda_z T} \iiint_{\text{wave product}} r\,dt = \frac{\omega}{2\pi\lambda_x\lambda_z} \int_0^T \int_0^{\lambda_x} \int_0^{\lambda_z} \Delta p \frac{\partial \xi}{\partial x} dx\,dz\,dt \qquad (2)$$

The following situations occurs due to the nature of the sign of the specific wave resistance, dR_x:

$$dR_x = \begin{cases} > 0; & \textit{Wave drag} \\ < 0; & \textit{Wave thrust} \end{cases}$$

Definition 6: Flutter Characteristic Parameter

The ratio of the average density of mechanical energy, dE, to the specific wave resistance, dR_x, characterizes the type of interaction between the flow and the vibrating surface. In this analysis this ratio is defined by flutter characteristic parameter, $\bar{\chi}$ (unit: ms^{-1}):

$$\bar{\chi} = \frac{dE}{dR_x}$$

The sign of the flutter characteristic parameter, $\bar{\chi}$, dictates the resulting mode of interaction between the flow and the vibrating surface. The possible modes of gasdynamic-elastic wall interaction are defined as follows:

$$\bar{\chi} = \begin{cases} < 0; & (dE > 0,\ dR_x < 0,) \Rightarrow \textit{wave thrust} \\ < 0; & (dE < 0,\ dR_x > 0) \Rightarrow \textit{panel flutter} \\ > 0; & (dE > 0,\ dR_x > 0) \Rightarrow \textit{wave drag} \\ > 0; & (dE < 0,\ dR_x < 0) \Rightarrow \textit{damping} \end{cases}$$

The ratio, $\bar{\chi}$, is negative in the case of wave thrust and panel flutter.

3. The Governing Differential Equations for Aeroelastic Problem

The key to solving the gasdynamic problem described above lies in finding appropriate solutions to equations (1) and (2). In this analysis the pressure disturbance, Δp, the wavelengths λ_x and λ_z, the frequency ω and the boundary function, ξ,

$$\xi = \xi(x,z,t)$$

are evaluated by solving the aeroacoustic or small disturbance equations with appropriate boundary conditions.

The propagation of small disturbances of pressure, Δp, temperature, ΔT, and velocity, Δu, of a uniform plane stream, traveling with average velocity V_∞ along the x-axis, is described by the equation[1]:

$$\left[\left(\frac{\partial}{\partial t} + V_\infty \frac{\partial}{\partial x}\right)^2 + a_\infty^2 \frac{\partial^2}{\partial x_n \partial x_n}\right]\psi = 0 \qquad (3)$$

where Ψ represents the following perturbed gasdynamic quantities in the form

$$\psi = \begin{cases} \dfrac{\Delta p}{\gamma p}; & p = p_{avg} + \Delta p \\ \dfrac{\Delta T}{(\gamma - 1)T}; & T = T_{avg} + \Delta T \\ -\dfrac{M_\infty^2}{V_\infty}\Delta u; & u = U_{avg} + \Delta u \end{cases} \qquad (4)$$

V_∞, a_∞, γ are the velocity, and the speed of sound in the free stream, and the ratio of specific heats. The summation index, n, $n = 1, 2, 3$; represents the coordinates x, y and z.

In the case of separation-free flow over an impermeable oscillating elastic surface, the following boundary condition holds:

$$\left(\frac{\partial}{\partial t} + V_\infty \frac{\partial}{\partial x}\right)^2 \xi + a_\infty^2 \frac{\partial \psi}{\partial y} = 0 \qquad (5)$$

Equations (3) through (5) form the governing system of differential equations (GDE) which describe the interaction of a parallel flow over a vibrating elastic surface. In this analysis the GDE will be solved for a special class of prescribed boundary functions.

4. Analytical Evaluation of the GDE for Plane Wave Boundary Conditions

It is assumed that the elastic surface performs forced oscillations and its transverse displacements are represented by plane waves in complex form,

$$\xi = B_1 e^{i\vartheta} + B_2 e^{i\vartheta} \qquad (6)$$

where

$$\vartheta = \left(\omega t + \frac{2\pi}{\lambda_x} x + \frac{2\pi}{\lambda_z} z \right)$$

Equation (6) represents the fixed form of vibration of the elastic boundary. However, the values of the amplitudes, B_1 and B_2, the frequency of oscillation ω and the wavelengths of a single rectangular wave pocket, λ_x and λ_z are dictated by the influence of the transverse gas flow. The parameters ω, λ_x and λ_z are determined by substituting equation (6) into (5) and subsequently solving the modified GDE for the function Ψ.

The disturbances of the gasdynamic parameters, Ψ, described in equations (4), that are caused by the vibratory motion and which satisfy the GDE is found as[2]

$$\psi = -i\left(jB_1 N \frac{2\pi}{\lambda_x} \right) e^{i\Omega} + i\left(jB_2 N \frac{2\pi}{\lambda_x} \right) e^{-i\Omega} \qquad (7)$$

where

$$\Omega = \left[\omega t + \frac{2\pi}{\lambda_x} x + j \frac{2\pi\sqrt{(L-1.0)}}{\lambda_x} y + \frac{2\pi}{\lambda_z} z \right],$$

$$i = \sqrt{-1}, \qquad L = \left(M_\infty - St_x\right)^2 - \left(\frac{\lambda_x}{\lambda_z}\right)^2,$$

$$N = \frac{\left(M_\infty - St_x\right)^2}{\sqrt{(L-1.0)}}$$

and

$$St_x = \pm \frac{\omega \lambda_x}{2\pi a_\infty}, \begin{cases} > 0 \Rightarrow \textit{Right running waves} \\ < 0 \Rightarrow \textit{Left running waves} \end{cases}$$

The symbol St_x is the Strouhal number and which is related to the mach number of the phase velocity of the displacement wave, traveling to the right and left along the x-axis, and j is the radiation parameter, which characterizes the direction of the disturbance propagation, either to or from the vibrating surface. The radiation parameter j is defined as follows:

$$j = \begin{cases} +1 \Rightarrow \textit{Radiation of Disturbances} \\ -1 \Rightarrow \textit{Absorbtion of Disturbances} \end{cases}$$

There is a discontinuity in the amplitude of the disturbances of the flow parameters for $L = 1$. This point is defined as the critical point[2]. Using $L = 1$ as reference the various regimes in the flow can be characterized as follows:

$$L = \begin{cases} > 1.0; & \textit{Supercritical region} \\ 1.0; & \textit{Critical point} \\ < 1.0; & \textit{Subcritical region} \end{cases}$$

In this analysis the boundary function, ξ, representing a chessboard type vibration pattern, and a single traveling wave of the elastic surface will be studied. In analyzing the proposed problems, the immediate task is to identify the parameters in the gas flow which are responsible for sustaining the vibrating motions and possible panel flutter. However, before an analysis is

conducted using the theory outlined in this section the solution, given in equation (7), will be validated.

4. Validation of the Analytical Solution in the Case of Steady flow Over a Wavy Wall

In this section the results of the gasdynamic interaction theory outlined in the previous section will be used to estimate the 2D steady flow properties over a wavy wall.

The geometry of the wavy surface is described by the boundary function,

$$\xi = h\cos\left(\frac{2\pi}{l}x\right) \qquad (8)$$

The analytical solution for flow over the wavy wall can be constructed under the following conditions: $\omega = 0$, $B_1 = B_2 = \frac{h}{2}$, $\lambda_x = l$ and $\lambda_z = \infty$.

Substituting these conditions into equation (7) results in

$$\Omega = \left[\frac{2\pi}{l}x + j\frac{2\pi\sqrt{\left(M_\infty^2 - 1.0\right)}}{l}y\right]$$

and

$$\psi = -i\left(j\frac{h}{2}\frac{M_\infty^2}{\sqrt{M_\infty^2 - 1.0}}\frac{2\pi}{l}\right)\left[e^{i\Omega} + e^{-i\Omega}\right]$$

The critical point for this aeroelastic problem occurs at sonic conditions. The subcritical and supercritical regimes are defined by the subsonic and supersonic regions in the flow field.

Subsonic Flow

In the case of subsonic flow, for $M < 1.0$, and with the appropriate surface radiation parameter, j, the perturbation quantities are found to be of the form,

$$\left.\begin{array}{c}\frac{\Delta p}{p}\\ \frac{\Delta T}{(\gamma-1)T}\\ -\frac{M_\infty^2}{V_\infty}\Delta u\end{array}\right\} = \frac{-2\pi h M_\infty^2}{l\sqrt{1.0 - M_\infty^2}} e^{\frac{-2\pi\sqrt{1.0-M_\infty^2}}{l}y}\cos\left(\frac{2\pi}{l}x\right) \qquad (9)$$

The amplitude of the perturbation quantities decrease exponentially with increasing distances from the plate. Besides, the results obtained upon the evaluation of equations (1) and (2) reveals that in the subcritical regime there is no energy exchange between the wall and the flow, ie., $dE = 0$, *and* $dR_x = 0$.

The relations in equation (9) can be used to reproduce the exact relationships for the perturbation velocity potential, ϕ, and the wall pressure coefficient, $C_{p,wall}$ in the form[3]:

$$\phi = \frac{hV_\infty}{\sqrt{1.0 - M_\infty^2}} e^{\frac{2\pi\sqrt{1.0-M_\infty^2}}{l}y}\sin\left(\frac{2\pi}{l}x\right) \qquad (10)$$

and

$$C_{p,wall} = \left(\frac{-4\pi h}{l\sqrt{1.0 - M^2}}\right)\cos\left(\frac{2\pi}{l}x\right) \qquad (11)$$

Supersonic Flow

Similarly, for supersonic flow, $M > 1.0$, and the appropriate surface radiation parameter, j, the perturbation quantities for the inviscid flow parameters are reduced to

$$\left.\begin{array}{c}\frac{\Delta p}{p}\\ \frac{\Delta T}{(\gamma-1)T}\\ -\frac{M_\infty^2}{V_\infty}\Delta u\end{array}\right\} = \frac{-2\pi h M_\infty^2}{l\sqrt{M_\infty^2 - 1.0}}\sin\left[\frac{2\pi}{l}\left(x - \sqrt{M_\infty^2 - 1.0}y\right)\right] \qquad (12)$$

In the supercritical regime the disturbances are pronounced through the

flow field. Evaluation of the integrals in equations (1) and (2) reveals that there is no energy exchange, ie., $dE = 0$, but the flow experiences wave drag,

$$dR_x = \frac{\pi h^2 M_\infty^2}{l\sqrt{M_\infty^2 - 1.0}}$$

In the case of supersonic flow, the relations in equation (12) can be used to reproduce the exact relationships for the perturbation velocity potential, ϕ, and the wall pressure coefficient, $C_{p,wall}$ in the form[3]:

$$\phi = \frac{-hV_\infty}{\sqrt{M_\infty^2 - 1.0}} \cos\left(\frac{2\pi}{l}x - \frac{2\pi\sqrt{M_\infty^2 - 1.0}}{l}y\right) \quad (13)$$

and

$$C_{p,wall} = \frac{-4\pi h}{l\sqrt{M_\infty^2 - 1.0}} \sin\left(\frac{2\pi}{l}x\right) \quad (14)$$

The results obtained in this section confirms the validity of the gasdynamic interaction theory outlined in the previous section.

5. Aeroelastic Response of Vibrating Surface with the Traveling Wave Mode of Vibration

Vibrations in the form of a traveling wave is considered an elementary mode of vibration of an elastic plate. All other modes of vibration can be considered a complex combination of right-running and left running waves. In the remainder of this paper the focus will be on two problems, namely, the aeroelastic response due to a single wave, and a combination of traveling waves.

Consider an elastic surface undergoing vibrations in the form of a right running wave. In this case the boundary function, ξ, takes the form

$$\xi = B\sin\left(\omega t + \frac{2\pi}{\lambda_x}x + \frac{2\pi}{\lambda_z}z\right) \quad (15)$$

An illustration of a traveling wave on the elastic wall is depicted in figure 2.

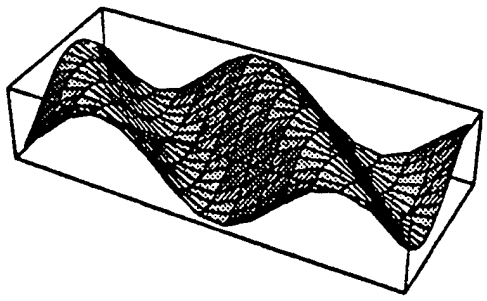

Figure 2: A Single Right running wave

The corresponding gasdynamic parameters in accordance with equation (7) is obtained in the form:

$$\psi = -jNB\frac{2\pi}{\lambda_x}\sin\left(\omega t + \frac{2\pi}{\lambda_x}x + \frac{2\pi}{\lambda_z}z\right) \quad (16)$$

The disturbance in the pressure is obtained as

$$\Delta p = (-j)\gamma p N \frac{\partial \xi}{\partial x}$$

where N is defined as follows:

$$N = \frac{\left(M_\infty - St_x\right)^2}{\sqrt{\left(M_\infty - St_x\right)^2 - \left(\frac{\lambda_x}{\lambda_z}\right)^2 - 1.0}}$$

The critical points are defined in terms of the Strouhal numbers, St_x, such that,

$$St_x = M_\infty \pm \sqrt{1.0 + \left(\lambda_x/\lambda_z\right)^2}$$

These two points separate three distinct regions in the flow field over the oscillating surface: Regimes *I*, *II*, and *III*.

Using the relationships (1) and (2) the values of the mechanical energy flux and the specific wave resistance, dE and dR are found in the forms:

$$dE = -j\gamma p N \frac{\omega \pi B^2}{\lambda_x}$$
$$dR = -j\frac{\gamma p}{2} N \left(\frac{2\pi B}{\lambda_x}\right)^2 \qquad (17)$$

Finally the flutter characteristic parameter, $\bar{\chi}$, is found in the form:

$$\bar{\chi} = \frac{\omega \lambda_x}{2\pi} \qquad (18)$$

In the subcritical region no exchange of energy occurs and the surface does not experience wave resistance. This phenomena is attributed to the fact that in the subcritical region the amplitude of the flow field small disturbance parameters decays exponentially with increasing distances from the vibrating surface. For $\omega > 0$, $dE > 0$, and $dR > 0$. In regime *III* the flow generates tractive force, while in region *I* wave drag is generated. However, in both regions, $\bar{\chi}$ is positive, therefore no panel flutter can be expected.

6. Aeroelastic Response of Vibrating Surface with the Chessboard Mode of Vibration

Consider the vibrating surface under the action of two traveling waves; namely a right and a left running wave. This mode of vibration yields a chessboard pattern. In this case the boundary function, ξ, takes the form,

$$\xi = B\cos(\omega t)\sin\left(\frac{2\pi}{\lambda_x}x\right)\cos\left(\frac{2\pi}{\lambda_z}z\right) \qquad (19)$$

For the chessboard wavy structure there exists two crests and two troughs in one rectangular wave packet with wavelengths λ_x and λ_z. An illustration of the chessboard mode of vibration is given in figure 3.

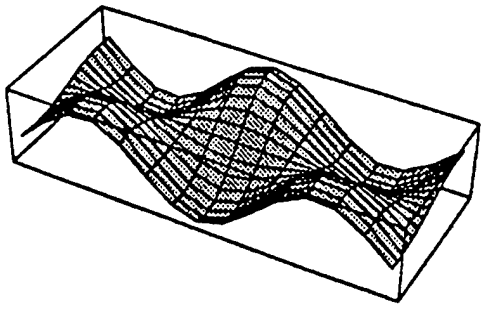

Figure 3: Chessboard Mode of Vibration

The corresponding perturbation quantities can be expressed in the form;

$$\left.\begin{matrix} \frac{\Delta p}{\gamma p} \\ \frac{\Delta T}{(\gamma-1)T} \\ -\frac{M_\infty^2}{V_\infty}\Delta u \end{matrix}\right\} = \frac{1}{2}\left\{\begin{matrix} \left[N^- - jN^+\right]\frac{\partial \xi}{\partial x} - \\ \frac{1}{a_\infty St_x}\left[N^- + jN^+\right]\frac{\partial \xi}{\partial t} \end{matrix}\right\} \qquad (20)$$

where

$$N^{\pm} = \frac{\left(M_\infty \pm St_x\right)^2}{\sqrt{\left(M_\infty \pm St_x\right)^2 - 1.0 - \left(\lambda_x/\lambda_z\right)^2}}$$

The upper sign is for right running waves and the lower sign is for left running waves. The critical points are defined by

$$St_{x\pm,critical} = M_\infty \pm \sqrt{1.0 + \left(\lambda_x/\lambda_z\right)^2} \qquad (21)$$

The resulting two singular points divides the flow field into three distinct regimes. In this analysis, these regions, labeled Regimes *I*, *II*, and *III*. Regime *I* and *III* make up the supercritical flow region such that,

Regime I: $St_{x-} < M_\infty - \sqrt{1.0 + \left(\lambda_x/\lambda_z\right)^2}$

Regime III: $St_{x+} > M_\infty + \sqrt{1.0 + \left(\lambda_x/\lambda_z\right)^2}$

Regime *II* defines the subcritical region, such that,

$$\textit{Regime II:}\quad St_{x-,critical} < St_x < St_{x+,critical}$$

Evaluating integrals (1) and (2) for the values of the mechanical energy flux, E, and the specific wave resistance, R_x results in the expressions:

$$dE = \frac{\gamma p}{16}\frac{2\pi\omega B^2}{\lambda_x}\left[N^- - jN^+\right]$$
$$dR_x = \frac{\gamma p}{16}\left(\frac{2\pi B}{\lambda_x}\right)^2\left[N^- + jN^+\right] \qquad (22)$$

The corresponding flutter characteristic parameter, $\bar{\chi}$, can now be expressed as

$$\bar{\chi} = \frac{\omega\lambda_x}{2\pi}\left(\frac{N^- - jN^+}{N^- + jN^+}\right) \qquad (23)$$

All the major expressions are evaluated and it is time to evaluate the physics of the resulting chessboard vibrations.

Subcritical Region

In the subcritical region, Regime *II*, $j = 0$, and the flutter characteristic parameter, $\bar{\chi}$, takes the form of

$$\bar{\chi} = \frac{\omega\lambda_x}{2\pi} > 0$$

Therefore no panel flutter can be expected in this region. Besides, in the subcritical region the amplitude, B, of vibration according to equation (6) are imaginary. Proceeding in a similar manner as in the case of the wavy wall, it can be shown that in this region that the flow disturbances will decay exponentially with increasing distance from the surface and no energy or force exchange occurs.

Supercritical Region

In order to determine the areas where $\bar{\chi}$ is negative it is necessary to analyze the amplitude function N, defined in equation (16). The chessboard mode of vibration is made up of a special combination of right and left running waves with identical phase velocity. A plot of the amplitude function, N in relation to the dimensionless vibration frequency, St_x (or Strouhal number) illustrating the right-running ($St_x > 0$) and left-running ($St_x < 0$) waves are indicated in figure 4. In generating figure 4 the Mach number, M and the ratio of the wave lengths, $\left(\lambda_x/\lambda_z\right)$, are taken as *0.3* and *1.0*, respectively.

Using the results indicated in figure 4 and the relationship (23) for the flutter characteristic, $\bar{\chi}$, it can be concluded that

$$\bar{\chi} = \begin{cases} > 0; \forall\, St_x, St_x \in (\textit{Regions E and R}) \\ < 0; \forall\, St_x, St_x \in (\textit{Regions E and R}) \end{cases}$$

The plot illustrated in figure 4 indicates that over the whole range of frequencies, ω, and modes $\left(\lambda_x/\lambda_z\right)$ of forced oscillations of the vibrating surface having the chessboard wavy structure mechanical energy flux, dE, must be supplied from the flow to maintain vibrations. Moreover, flutter is only possible in the neighborhood of the critical points: These critical zones are indicated in figure 4 as zones E and R for which

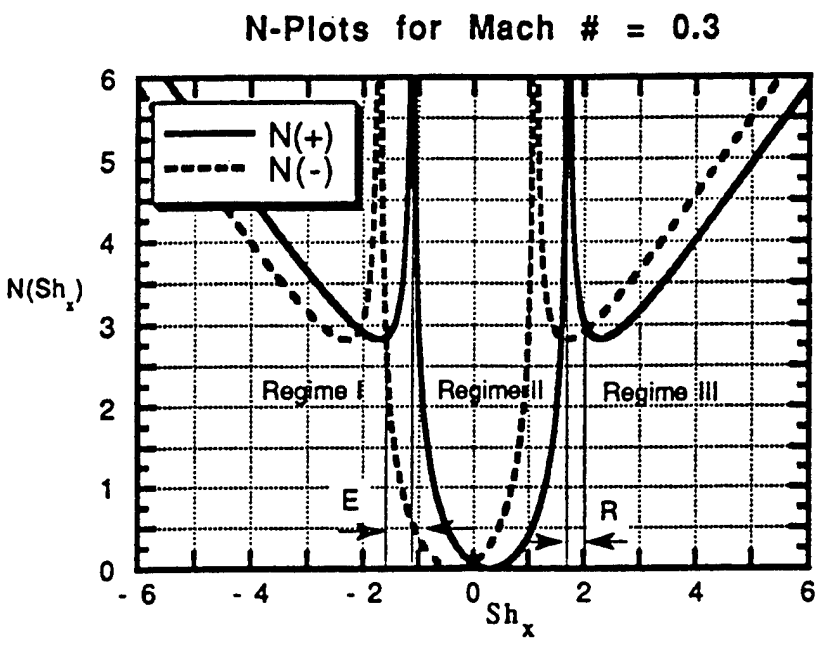

Figure 4. Plot of Amplitude, N, vs. Strouhal Number, St_x

$$\begin{matrix} \textit{Regime I} \\ j = 1 \\ N^- < N^+ \end{matrix} \Rightarrow \begin{cases} dE < 0 \\ dR_x > 0 \end{cases} \Rightarrow \bar{\chi} < 0$$

and

$$\begin{matrix} \textit{Regime III} \\ j = -1 \\ N^- > N^+ \end{matrix} \Rightarrow \begin{cases} dE > 0 \\ dR_x < 0 \end{cases} \Rightarrow \bar{\chi} < 0$$

A detailed analysis[2] of regions E and R showed that panel flutter can be expected for Strouhal number, St_x, in the range of

$$E: \quad St_{x-,flutter} \in (St_{x,critical} - \varepsilon^-, \quad St_{x,critical})$$

$$R: \quad St_{x+,threat} \in (St_{x,critical}, \quad St_{x,critical} + \varepsilon^+)$$

where ε is found in the form[2]

$$\varepsilon^{\pm} = \frac{\left(1+\left(\lambda_x/\lambda_z\right)^2\right)^{3/2}}{8M_\infty\left[M_\infty \pm \sqrt{1+\left(\lambda_x/\lambda_z\right)^2}\right]} \qquad (24)$$

In the critical zone, E, in regime *I*, energy is taken from the flow, $dE < 0$, and wave resistance is encountered, i.e. $dR_x > 0$. Only in this narrow zone, where energy is transmitted from flow to elastic surface is panel flutter possible. On the other hand, in regime *III* tractive force, $dR < 0$ is encountered while energy is supplied from the flow, $dE > 0$, to maintain vibratory motion.

7. Flat Plate Flutter Frequency

Consider the case of a flat plate undergoing the chessboard mode of vibration. Assume that wave numbers, m and n can be described by

$$L_x = \frac{m}{2}\lambda_x$$

$$L_z = \frac{n}{2}\lambda_z$$

where L_x and L_y are the length and width of the plate. Then, based on the theory described in this analysis the Strouhal number, St, at which panel flutter is expected can be found using the relationship

$$St_{flutter} = M_\infty - \sqrt{1.0 + \left(mL_x / nL_z\right)^2} - \varepsilon \quad (25)$$

8. Experimental Findings

In this section a qualitative analysis is conducted on the vibratory modes of engine struts and their relation to panel flutter.

Experimental findings[4] showed that the typical modes of vibrations of engine front frame panel can be illustrated in the form of contour plots as depicted in Appendix A, figures A1 and A2. Based on the aeroelastic theory[5] described herein, two classes of panel vibratory modes in the form of contour plots were sought, namely, a class of modes that result in panel flutter, and class of vibratory modes that does not lead to flutter. Contour plots representing the vibratory modes that does and that does not lead to flutter are illustrated in figures 5 and 6.

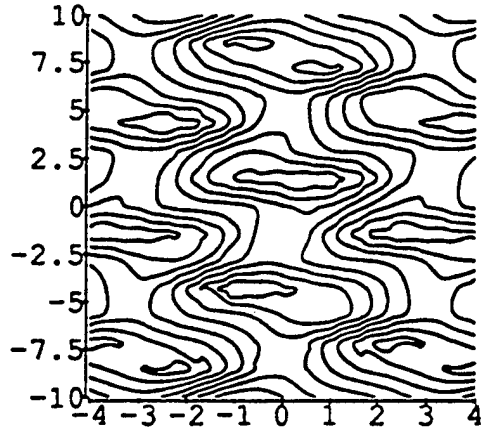

Figure 5: Contour plot of flutter modes

The observed modes of vibration of the engine front frame struts, as illustrated in figures 5 and 6, fall into the class of modes which can result in structural instabilities.

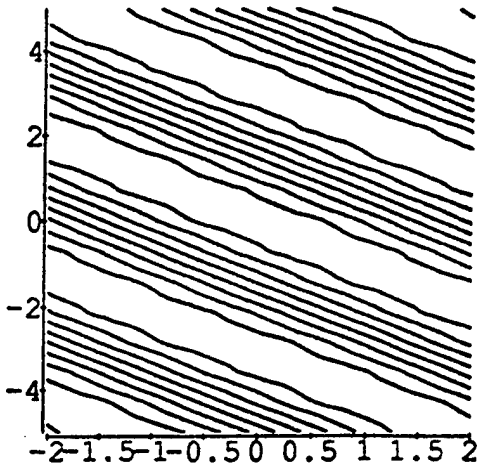

Figure 6: Contour plot of stable modes

9. Conclusions

The analytical model used in this analysis to evaluate the interaction between a gas flow and a vibrating wall has the capability of reproducing the exact solution of the small disturbance equations. It was demonstrated that panel flutter parameter is a function of the Strouhal number, St, and the mode of vibration of the elastic surface. This analysis showed that for a single traveling wave flutter is impossible. However, for more complex modes of vibration which are made up of a combination of traveling waves traveling waves, such as the chessboard pattern, flutter can and does occur. Furthermore, panel flutter is not limited to supersonic flow, but to a narrow band of frequencies, ω, or Strouhal number, St, in the supercritical regions.

In the subcritical region the amplitude of disturbances of the flow parameters decay exponentially with increasing distances from the vibrating surface. As a result the flow in the subcritical flow regime *II* does not on the average exchange energy with the vibrating surface and does not experience wave resistance.

The flutter analysis conducted in this study is based on inviscid

aerodynamics. In the case of viscous flow over the vibrating surface a boundary layer is encountered. If the depth of the boundary layer, δ, approximates the stationary wave length λ_x or λ_z, and the effective Mach number $M_{effective}$ close to the vibrating surface becomes less than the Mach number in the outer inviscid gas stream then the result may be an expansion of the range of frequencies for which flutter can occur.

10. Reference

1. Bisplinghoff, R. L., Holt, A., "Principles of Aeroelasticity," Dover Publications, Inc., New York, 1975.
2. Sergienko, A. A., Gasdynamic interaction between flow and vibrating shell, Izvestiya VUZ. Aviatsionnaya Tekhnika, Vol. 34, No. 1, pp. 15-19, 1991.
3. Anderson, John, D., "Modern Compressible Flow with Historical Perspective," McGraw-Hill Series in Mechanical Engineering.
4. Baker, A. J., "Noncontacting vibration measurement: role in design and industrial applications." Tech. Review, March 1990.
5. AEDAR Internal Report, No. AIR-3-AERO-9-93.

Appendix A

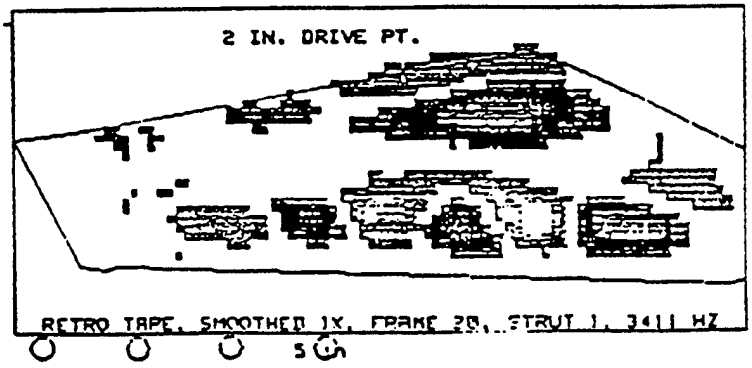

Figure A1: Experimental observation of engine strut vibration mode, Ref. 4.

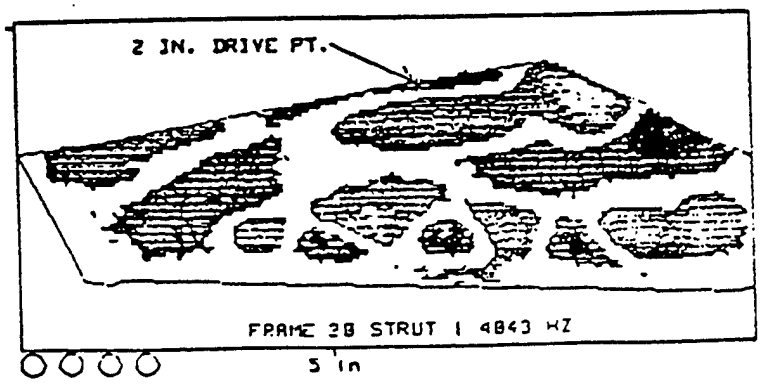

Figure A2: Experimental observation of engine strut vibration mode, Ref. 4.